JOURNAL OF NEUROPHYSIOLOGY
Vol. 64, No. 1, July 1990. *Printed in U.S.A.*

Spatial and Temporal Response Properties of Lagged and Nonlagged Cells in Cat Lateral Geniculate Nucleus

A. B. SAUL AND A. L. HUMPHREY
Department of Neurobiology, Anatomy, and Cell Science, University of Pittsburgh School of Medicine, Pittsburgh, Pennsylvania 15261

SUMMARY AND CONCLUSIONS

1. It has recently been shown that the X- and Y-cell classes in the A-layers of the cat lateral geniculate nucleus (LGN) are divisible into lagged and nonlagged types. We have characterized the visual response properties of 153 cells in the A-layers to *1*) reveal response features that are relevant to the X/Y and lagged/nonlagged classification schemes, and *2*) provide a systematic description of the properties of lagged and nonlagged cells as a basis for understanding mechanisms that affect these two groups. Responses to flashing spots and drifting gratings were measured as the contrast and spatial and temporal modulation were varied.

2. X- and Y-cells were readily distinguished by their spatial tuning. Y-cells had much lower preferred spatial frequencies and spatial resolution than X-cells. Within each functional class (X or Y), however, lagged and nonlagged cells were similar in their spatial response properties. Thus the lagged/nonlagged distinction is not one related to the spatial domain.

3. In the temporal domain X- and Y-cells showed little difference in temporal tuning, whereas lagged and nonlagged cells showed distinctive response properties. The temporal tuning functions of lagged cells were slightly shifted toward lower frequencies with optimal temporal frequencies of lagged X-cells averaging an octave lower than those of nonlagged X-cells. Temporal resolution was much lower in lagged X- and Y-cells than in their nonlagged counterparts.

4. The most dramatic differences between lagged and nonlagged cells appeared in the timing of their responses, as measured by the phase of the response relative to the sinusoidal luminance modulation of a spot centered in the receptive field. Response phase varied approximately linearly with temporal frequency. The slope of the phase versus frequency line is a measure of total integration time, which we refer to as visual latency. Lagged cells had much longer latencies than nonlagged cells.

5. The intercept of the phase versus frequency line is a measure of when in the stimulus cycle the cell responds; we refer to this as the intrinsic or absolute phase of the cell. This measure of response timing not only distinguished lagged and nonlagged cells well but also covaried with the sustained or transient nature of cells' responses to flashed stimuli. Absolute phase lagged the stimulus for lagged cells, led the stimulus for nonlagged cells, and approached a quarter-cycle phase lead or lag for cells that responded transiently.

6. We conclude that geniculate X- and Y-cells are distinguished by their spatial but not temporal response properties; these characteristics are largely inherited from the retina. On the other hand, lagged and nonlagged cells are indistinguishable spatially but differ temporally. These temporal differences reflect intrageniculate mechanisms and indicate that the LGN performs a major role in the temporal transformation of signals passing from retina to cortex.

7. The responses of virtually all cells to square-wave flashing stimuli could be predicted from their responses to sinusoidal stimuli by the use of response phase data and assuming linear summation. The inhibitory dip and anomalous offset discharge that characterize the responses of lagged cells to flashed stimuli are present in these linear predictions. Thus it is not necessary to invoke strong nonlinearities in the temporal domain to account for the response profiles of lagged and nonlagged geniculate cells or for sustained and transient firing patterns.

8. Lagged and nonlagged cells responded approximately one-quarter cycle apart at low temporal frequencies. Because of the latency difference between these cell types, this quarter-cycle phase difference was maintained only over a limited range of frequencies. This range roughly matched the tuning width of lagged cells, so that lagged cells tended to cease responding around the point where their responses would be a half cycle out of phase with nonlagged cells of the same center sign. We suggest that the response timing differences between lagged and nonlagged cells may be important for generating direction selectivity in visual cortex.

INTRODUCTION

Cat visual cortical cells display remarkable response properties in light of their relatively simple inputs from the lateral geniculate nucleus (LGN). Specificity for a variety of stimulus dimensions arises in cortex out of a seemingly homogeneous collection of geniculate neurons. The dominant projections to *area 17* arise from X- and Y-cells in the geniculate A-laminae (Humphrey et al. 1985; Malpeli 1983; Stone and Dreher 1973). These cells inherit their receptive fields largely unaltered from their retinal inputs (Cleland et al. 1971; Hoffman et al. 1972). Little evidence had accumulated for significant geniculate processing of visual information until the discovery of lagged X-cells (Mastronarde 1987a,b). These geniculate cells differ from their retinal X-afferents and from adjacent, nonlagged, geniculate X-cells in displaying an early inhibition rather than excitation to the onset of a visual stimulus in their receptive field. This early inhibition produces a delayed latency to discharge. Based on structural and functional evidence, it is hypothesized that intrageniculate inhibitory interneurons are responsible for generating the lagged-X response profile (Humphrey and Weller 1988b; Mastronarde 1987a). Both lagged and nonlagged X-cells project to visual cortex in substantial numbers, and it is estimated that the cells comprise ~40 and 60%, respectively, of the geniculocortical X-afferents (Humphrey and Weller 1988b).

Our understanding of the geniculate mechanisms that underlie lagged and nonlagged X-cells, as well as the impli-

cations for cortical function, require further details about how these cells respond to visual stimuli. Previous reports suggested that the two groups of X-cells are similar in such spatial properties as handplotted receptive field–center size and spatial resolution (Humphrey and Weller 1988a; Mastronarde 1987a). In the temporal domain, it was shown that lagged X-cells prefer lower temporal frequencies (Humphrey and Weller 1988a) and slower speeds than nonlagged X-cells and that the responses to moving bars occur much later in lagged than in nonlagged cells (Mastronarde 1987a). Taken together, the previous evidence suggested strongly that the differences between lagged and nonlagged X-cells were of a temporal rather than spatial nature. In the present work we have investigated this issue more systematically than heretofore, both to validate previous findings and to extend the analyses in the temporal and contrast domains. We have also extended these analyses to the newly recognized (Mastronarde 1988a) group of lagged Y-cells.

We found that, within each cell class (X or Y), lagged and nonlagged cells were indistinguishable spatially. The clearest differences existed in the temporal domain. In exploring the temporal properties of geniculate cells, it became clear that not only the lagged/nonlagged distinction, but also the transient/sustained distinction and other aspects of the timing of visual responses, could be simply related to measurements of the phase of responses to sinusoidally modulated stimuli. A simplifying assumption of linear temporal summation appears to be a reasonable approximation for geniculate A-layer cells. This implies, in particular, that the mechanisms responsible for the peculiar responses of lagged X-cells transform the retinal input linearly. In addition, if cortex were to combine geniculate inputs even quasi-linearly, direction selectivity could be generated out of the responses of lagged and nonlagged cells.

These results have been presented previously in abstract form (Saul and Humphrey 1988, 1989).

METHODS

Physiological preparation

The general methods for surgical preparation, visual and electrical stimulation, and recording are described in detail in Humphrey et al. (1985). Adult cats were anesthetized with the use of 4% halothane in nitrous oxide and oxygen. A radial vein was cannulated, and an endotracheal tube was inserted. After placement in a stereotaxic frame, paralysis was induced with an intravenous injection of gallamine triethiodide (Flaxedil), and the animal was henceforth ventilated artificially at a rate sufficient to maintain end-tidal CO_2 at ~4%. The gas mixture contained ~70% N_2O and 30% O_2 with 1–2% halothane for the duration of surgical procedures. Rectal temperature was maintained at ~37.5°C with a thermostatically controlled heating pad. Heart rate was monitored throughout the experiment as one indicator of physiological state. An intravenous infusion containing 3.6 mg/h of Flaxedil, 0.7 mg/h of *d*-tubocurarine, and 1 $mg \cdot kg^{-1} \cdot h^{-1}$ of pentobarbital sodium (Nembutal) in 5% dextrose and lactated Ringer solution was given continuously at a rate of ~6 ml/h. Craniotomies were made over the optic chiasm and the LGN for placement of bipolar stimulating electrodes and recording electrodes, respectively.

Care was taken to ensure proper anesthetic levels throughout the experiment. All incision and pressure points were infiltrated with 2% lidocaine HCl. The head was supported nontraumatically in the stereotaxic by a crossbar attached to screws inserted into the skull, which allowed removal of the ear and eye bars. The electroencephalogram (EEG) was recorded continuously, and small boluses (3–6 mg) of Nembutal were administered intravenously, if necessary. This maintained a state of strong EEG synchronization and barbiturate spindling during surgery and mild synchronization with no spindling during recording (Hammond 1978; Humphrey and Weller 1988a).

The pupils were dilated with atropine, and phenylephrine HCl was applied to retract the nictitating membranes. The corneas were covered with contact lenses fitted with 3-mm artificial pupils, and the eyes were flushed periodically with 1.5% saline to maintain optical quality. Refraction was evaluated by retinoscopy, and contact lenses were chosen to focus the eyes at a distance of 57 cm. The optic disks were projected onto a tangent screen at 114 cm, and the direction of gaze was estimated therefrom (Bishop et al. 1962).

Recording and electrical stimulation

Single neurons were recorded with tris(hydroxymethyl)aminomethane (Tris) glass micropipettes filled with 0.2 M KCl in Tris buffer and beveled to obtain impedances of 50–100 MΩ in vivo. As reported previously (Humphrey and Weller 1988a), moderately high-impedance electrodes are required to sample the small, lagged X-cells in the LGN. Lagged cells may also be recorded with tungsten-in-glass electrodes having small tip exposures (Heggelund and Hartveit 1989; Mastronarde 1987a). We repeatedly fail to record lagged cells with micropipettes filled with 3 M KCl, while consistently recording 2–3 lagged cells per penetration with similar pipettes filled with 0.2 M KCl. We speculate that the lower molarity reduces the sampling window of the pipettes and somehow allows better isolation of small amplitude potentials from the small lagged cells without interference from surrounding potentials generated by larger cells. The location of the electrode tip in the LGN was established with the use of Sanderson's (1971) maps, potentials evoked by chiasm stimulation, and cell ocular dominance. Single neurons in the A-layers were well isolated by the high-impedance electrodes, and somatic spikes were distinguished from axon spikes by their biphasic potentials and by the slow decay of axonal potentials. Latencies to electrical stimulation of the optic chiasm were measured from the foot of the action potential, taking the shortest consistent latency to repeated chiasm shocks (Humphrey and Weller 1988a).

General visual stimulation and identification of X- and Y-cells

Receptive fields were plotted initially by hand on a tangent screen 114 cm from the eyes. All subsequent visual stimulation was done with the use of a Tektronix 608 monitor 57 cm from the eye, driven by a Picasso image synthesizer (Innisfree, Cambridge MA) linked to an LSI-11/73 computer. The CRT subtended ~10° visual angle. All stimuli were presented monocularly with the nondominant eye occluded.

Cells were identified as X or Y primarily by the linearity of their spatial summation to counterphasing sine-wave gratings, as determined by Fourier analysis of their peristimulus time histograms (PSTHs) (Enroth-Cugell and Robson 1966). Gratings were modulated at 1 or 2 Hz, and the spatial frequency was slowly increased. If a spatial frequency could be found where the response component at the second harmonic of the stimulus temporal frequency exceeded twice the magnitude of the first harmonic component, the cell was classified as nonlinear and there-

fore Y (Hochstein and Shapley 1976). Cells with a second to first harmonic ratio <2.0 were identified as X (the ratio was usually <1.0).

Secondary, qualitative features of the cells supported our primary identification. All cells with optic chiasm latencies >1.7 ms or <1.4 ms were identified on the basis of spatial summation as X or Y, respectively, in agreement with previous reports (Humphrey and Weller 1988a; Wilson et al. 1976). Also, when matched for eccentricity, X-cells had smaller handplotted receptive fields than Y-cells, and most X-cell receptive-field surrounds displayed moderate to strong antagonism of the center, whereas those of most Y-cells did not. For a few cells (<5% of the sample), the linearity test yielded equivocal results, because of poor or erratic responses at high spatial frequencies. In these cases, the secondary criteria were used to identify cell class but only if all criteria agreed. If not, the cells remained unclassified and were excluded from the present analyses.

Stimulus protocols

The following tests were used to characterize the cells' visual response properties.

RESPONSES TO FLASHING SPOTS. A cell was identified as lagged or nonlagged by its response to a flashing spot centered in its receptive field (Humphrey and Weller 1988a). The luminance of the spot was modulated in a four-part cycle consisting of steps at 15, 25, 35, and 25 cd/m^2, with the background luminance constant at 25 cd/m^2. Each step lasted either 0.5 or 1.0 s. These 2- or 4-s cycles were repeated 50–200 times to generate a PSTH (Fig. 1).

SPATIAL RESPONSE PROPERTIES. The spatial response properties and spatial structure of the receptive fields of the geniculate cells were determined with the use of drifting sine-wave gratings of various spatial frequencies. Vertically oriented gratings drifting rightward across the receptive field at the preferred drift rate for each cell were presented for 10-s trials. Grating contrast was 0.4, and mean luminance was 25 cd/m^2. Seven to 10 spatial frequencies were tested, usually ranging from 0.125 to 2 cycles per degree (cpd) in approximately half-octave steps. Each frequency was randomly presented five times to generate a PSTH. At a typical drift rate of 2 Hz, each histogram was built from 100 stimulus cycles.

TEMPORAL RESPONSE PROPERTIES. The temporal response properties of cells were determined mainly by the use of the same spot as in the flashing spot test but now modulated sinusoidally between 15 and 35 cd/m^2 around a background luminance of 25 cd/m^2. Temporal frequencies of 0.5–24 Hz were typically tested with each frequency presented five times for 10 s each to generate a PSTH showing the average response over a stimulus cycle. Occasionally, cells were additionally tested at frequencies between 0.1 and 2 Hz to study their low-frequency behavior. The responses of the cell were timed relative to the luminance of the spot to determine the phase of the response relative to the stimulus.

Temporal response functions for some cells were also tested with drifting sine-wave gratings of optimal spatial frequency and contrast of 0.4. Responses were timed relative to a stimulus-cycle marking signal, but because the position of the grating relative to the cell's receptive field could not be easily determined, the response phase includes an unknown offset. Although this offset could be discovered by varying spatial frequency (Lee et al. 1981a), this method was not routinely used because of time constraints.

Eye movements occasionally introduced variability in response amplitudes during a test. When activity seemed affected, the data were rejected, and the stimulus was recentered before starting another run. The diameters of spot stimuli were chosen to be just smaller than the receptive-field center as plotted by hand to minimize the effect of eye-position drifts.

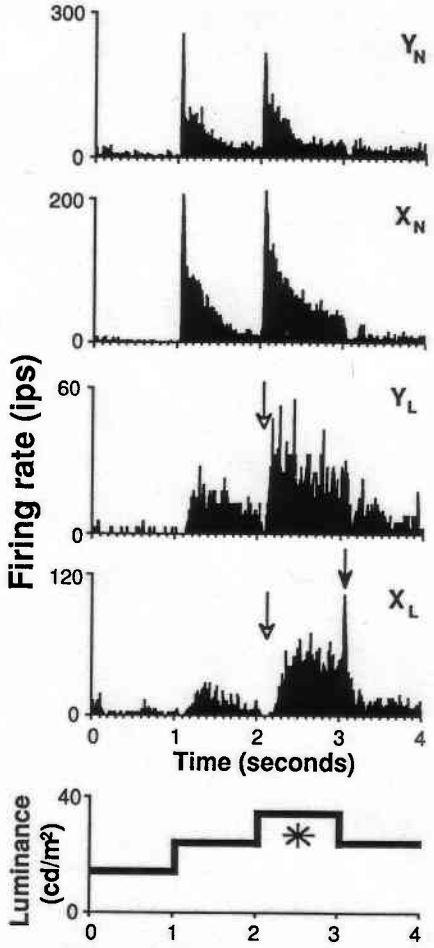

FIG. 1. Peristimulus histograms of responses from 4 ON-center geniculate neurons to the 4-part flashing spot stimulus. Stimulus was a small spot whose luminance was modulated as shown at *bottom*. For each cell, spot size was slightly smaller than the handplotted receptive-field center. Background luminance was 25 cd/m^2, matching the spot luminance from 1–2 s and 3–4 s. Star marks the luminance step most appropriate for stimulating these ON-center cells. Open arrows point to inhibitory dips in the Y_L- and X_L-cells, and filled arrow points to the anomalous offset discharge in the X_L-cell. Half-rise latencies for the Y_N-, X_N-, Y_L-, and X_L-cells were 39, 63, 156, and 320 ms, respectively. For half-fall, they were 23, 46, 117, and 132 ms, respectively.

Data analysis

Occurrence of action potentials was timed with millisecond resolution relative to stimulus events. All visual stimuli controlled by the computer were periodic, and spikes incremented histogram counters across one stimulus cycle. Binwidths varied with stimulus period but were generally <5 ms. Responses to sinusoidally varying stimuli were analyzed by converting the spike counts to firing rates per stimulus cycle and then Fourier analyzing the histogram to obtain the response component at the stimulus temporal frequency (and its harmonics). All Fourier transforms were performed with a standard Fast Fourier Transform (FFT) routine (Press et al. 1986). Visual latencies to the four-part flashing stimulus were measured as described by Humphrey and Weller (1988a).

Standard curves (e.g., difference of gaussians) were fit to response data. All fits minimized mean-squared error. Nonlinear

fits were found via a downhill simplex method (Nelder and Mead 1965; Press et al. 1986). Population results will be presented as arithmetic means plus or minus SEs unless otherwise specified. Unless otherwise specified, comparisons between means were based on one-tailed *t* tests. Correlations between variables were made within each cell classification with the use of linear (Pearson's) correlation.

RESULTS

Overview

Our results are derived from 153 X- and Y-cells recorded extracellularly in laminae A and A1 of the LGN. Among the X-cells, 81 were further identified as nonlagged or partially lagged and 33 as lagged. Among Y-cells, 32 and 7 were identified as nonlagged and lagged, respectively. All neurons had receptive fields within 35° of the area centralis; 55% of these were located within the central 10°. Approximately equal numbers of ON- and OFF-center cells were recorded in each cell group. The differences between ON- and OFF-center cells were not notable, leading us to combine them in the results presented here. We will first summarize how each neuron was identified as lagged or nonlagged by its response to flashing spots. We will then describe the spatial and temporal response properties of the cells as determined with the use of spots and gratings. We will show that the responses to sinusoidally modulated stimuli predict the responses to the flashing spot stimuli; that is, we will compare the frequency-domain and the time-domain response characteristics of the geniculate neurons. Finally, we will summarize our observations on the contrast-response properties of these cells.

Flash responses and identification of lagged and nonlagged cells

Figure 1 illustrates the response profiles of four representative ON-center cells to the four-part flashing spot stimulus. Each stimulus cycle evokes responses to two luminance steps. Although we focus our analysis on the portion of the histogram corresponding to the cell's center sign (bright for ON-center cells and dark for OFF-center cells), the immediately preceding luminance step is important because it raises the cell's firing above background levels so that any dip in discharge at stimulus onset can be detected.

The response profiles of the two cells at the *top* of the figure are characteristic of nonlagged geniculate neurons (Humphrey and Weller 1988a; Mastronarde 1987a). At spot onset, both gave a brisk transient discharge followed by a variably sustained firing that was stronger for the second cell than for the top cell. At spot offset, both cells quickly ceased discharging and returned to base-line firing. As indicated in the figure, we refer to these cells as Y_N and X_N. Our X_N-cells probably include neurons classified as X_S, X_M, and X_I by Mastronarde (1988b), with the majority probably corresponding to the more prevalent X_S, or single-input nonlagged X-cells.

In contrast to the brisk excitatory responses of the nonlagged cells, the lagged Y- and X-cells shown below responded sluggishly. Spot onset elicited an inhibitory dip in their discharge (open arrows) rather than an excitatory transient. Cell discharge was delayed because of the early dip, but once established it was sustained throughout the stimulus onset step. At spot offset, the cell at the *bottom* gave a transient anomalous offset discharge (filled arrow), which delayed the cell's return to background firing. Lagged X- and Y-neurons will be referred to as X_L and Y_L (Humphrey and Weller 1988a; Mastronarde 1987a, 1988a).

Most geniculate cells can be identified qualitatively as lagged or nonlagged by the shapes of their response profiles to flashing spots. As previously reported (Humphrey and Weller 1988a; Mastronarde 1987a; 1988a), they can also be distinguished quantitatively with the use of two measures: *1*) the *latency to half-rise*, which is sensitive to the inhibitory dip at stimulus onset, and *2*) the *latency to half-fall*, sensitive to the anomalous offset discharge at stimulus offset. The distributions of half-rise and half-fall latencies for our total sample are shown in Fig. 2. With the use of the criteria of Humphrey and Weller (1988a), cells with half-rise latencies <70 ms and half-fall latencies <60 ms were identified as nonlagged (filled squares and circles). Cells with half-rise latencies >100 ms and half-fall latencies >60 ms were identified as lagged (open squares and circles). All cells could be distinguished as lagged or nonlagged by these criteria with the exception of four X-cells that responded in all regards like X_N-cells (no inhibitory dip or anomalous offset discharge, short half-fall latency) but which had slightly longer (78–110 ms) half-rise latencies. We refer to these cells as partially lagged (X_{PL}) in accord with Mastronarde (1987a). Two Y-cells that had clear inhibitory dips and long half-rise latencies were classified as lagged (Y_L) despite their half-fall latencies of zero. The firing in these two cells had returned to background levels before spot offset.

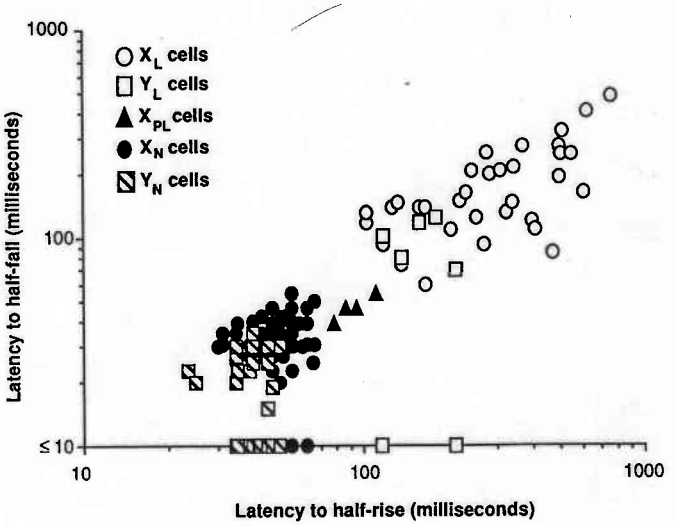

FIG. 2. Measured latencies to half-rise and half-fall from flash responses are plotted for all 153 cells recorded, although many of the nonlagged cells are obscured because of overlap. Half-rise reflects the latency at which the cell attained half-maximal firing after stimulus onset (Humphrey and Weller 1988a). Half-fall reflects the time taken for firing to decay by one-half after stimulus offset. Cells for which half-fall latencies could not be computed because too little activity was present just before stimulus offset are plotted on the horizontal axis in the ≤10-ms category. Open symbols identify lagged cells; filled symbols identify nonlagged cells or X_{PL} cells.

Figure 2 confirms previous observations that half-rise and half-fall latencies distinguish X_L- from X_N-cells and extends the findings to Y-cells. Within the lagged and nonlagged groups, Y-cell latencies overlapped those of X-cells, although they were significantly shorter, on average, than their X-cell counterparts ($P < 0.005$ for both groups, Mann-Whitney U test). Curiously, the separation between lagged and nonlagged X-cells exceeds that previously reported by Humphrey and Weller (1988a) with the use of similar measures. This is due mainly to the longer latencies of X_L-cells in the present study. The reasons for this are unclear. Nevertheless, the important point is that lagged and nonlagged X- and Y-cells can be easily identified with the use of the flashing-spot stimulus.

Two other features of the flash responses were measured: maximum discharge rate and transient/sustained behavior (quantified by the ratio of mean to maximum firing rate, equivalent to the Percent Area of Discharge reported by Humphrey and Weller 1988a). Maximum firing rates in X_N- and Y_N-cells were similar (131 and 146 spikes/s, respectively) and dwarfed the rate for X_L- and Y_L-cells (38 spikes/s for both). The four X_{PL}-cells averaged 48 spikes/s, more similar to the X_L- than to the X_N-cells. With regard to the transient/sustained distinction, smaller values of the ratio of mean to maximum firing rates correspond to more transient firing patterns. X_N-cells ranged widely in their sustained/transient character (mean ratio of 38 with a SD of 16), whereas Y_N-cells tended to be very transient (17 ± 12). X_L-cells had sustained responses (62 ± 10). The seven Y_L-cells varied considerably (42 ± 16) but were much more sustained than a typical Y_N-cell. By this measure, too, the four X_{PL}-cells resembled X_L-cells with an average ratio of 62.

Having identified cells physiologically, we next explored their response properties in the spatial, temporal, and contrast dimensions with regard to these classifications. We were particularly interested in the extent to which X- and Y-cells on the one hand, and lagged and nonlagged cells on the other hand, differ in their spatial and temporal tuning.

Spatial responses

The spatial response properties of the geniculate cells were characterized conventionally (Enroth-Cugell and Robson 1966; Rodieck 1965; So and Shapley 1981). For a range of 7–10 spatial frequencies presented to each cell, the fundamental response component was plotted against spatial frequency, and these data points were fit by a difference of gaussians function (representing the summed effects of an excitatory center and an inhibitory surround) to obtain four parameters that describe the cell's spatial tuning. Estimates of preferred spatial frequency and spatial resolution (the frequency above the optimum that would evoke 10% of the maximal response) were derived, as well as a set of parameters that describes the receptive field in the spatial domain. These numbers include estimates of the receptive-field center and surround sizes (r_c and r_s) and strengths (C and S, which are combined in the ratio S/C for normalization). Table 1 lists means obtained for several of these parameters for each cell group. We include in this table mean receptive-field *diameters* as measured by hand, and the receptive-field *radius* derived from the point where the center and surround strengths are equal. Note that the handplotted fields are about one-half the size of the fields derived from the drifting grating data.

We found that spatial tuning as measured by first harmonic responses differed markedly between geniculate X- and Y-cells, as previously reported (So and Shapley 1981). Y-cells generally responded best to the lowest spatial frequency tested (0.125 cpd), which excludes analysis of their relatively negligible surrounds. Y-cells had lower preferred spatial frequencies, lower spatial resolution, and larger receptive-field centers than X-cells when matched for eccentricity. All of these differences were highly significant ($P < 0.001$ for all applicable comparisons). Although our conclusions regarding X/Y differences agree with previous studies, our cells had lower spatial resolution and larger receptive field–center sizes than those previously reported. These differences might be partly explained by our use of constant (0.4) contrast stimuli and cutoffs at 10% of the peak, as opposed to contrast sensitivity measurements. Other differences in sampling, analysis, and anesthesia may play a role in these discrepancies.

Although there were clear differences between X- and Y-cells in spatial tuning, within each cell class lagged and nonlagged cells did not differ. Y_L-cells had receptive fields as large as Y_N-cells and matched their low-pass spatial fre-

TABLE 1. *Spatial receptive field parameters*

Cell Type	Eccentricity, deg	S/C	r_c, deg	r_s, deg	RF_{rad}, deg	RF_{size}, deg	SF_{opt}, cpd	Resolution, cpd
X_L								
Mean ± SE	9.8 ± 1.3 (33)	0.82 ± 0.10 (7)	0.47 ± 0.09 (9)	0.79 ± 0.15 (7)	0.54 ± 0.05 (8)	0.58 ± 0.06 (33)	0.50 ± 0.09 (9)	1.51 ± 0.21 (9)
Range	1–35	0.4–1.0	0.3–1.1	0.3–1.4	0.3–0.8	0.2–1.8	0.2–1.0	0.5–2.5
X_N								
Mean ± SE	10.9 ± 1.0 (77)	0.77 ± 0.07 (23)	0.40 ± 0.04 (24)	1.13 ± 0.12 (23)	0.63 ± 0.05 (23)	0.70 ± 0.04 (77)	0.43 ± 0.04 (24)	1.63 ± 0.17 (24)
Range	1–36	0.2–1.9	0.1–1.0	0.5–2.8	0.2–1.3	0.2–2.0	0.1–0.7	0.5–4.5
Y_L								
Mean ± SE	12.7 ± 2.4 (7)		2.2 ± 0.4 (3)			1.1 ± 0.3 (7)	0.13 ± 0.01 (4)	0.29 ± 0.03 (3)
Range	4–21		1.9–2.6			0.5–2.5	0.1–0.2	0.3–0.4
Y_N								
Mean ± SE	13.8 ± 1.4 (32)		1.47 ± 0.19 (12)			1.58 ± 0.17 (32)	0.12 ± 0.01 (12)	0.41 ± 0.05 (12)
Range	4–41		0.7–3.0			0.3–3.5	0.02–0.2	0.2–0.7

Number of cells tested in parentheses. S/C, ratio of surround to center strength; r_c and r_s, center and surround radii from difference of gaussians, respectively; RF_{rad}, receptive field radius derived from difference of gaussians; RF_{size}, subjectively measured receptive field diameter; SF_{opt}, optimal spatial frequency; resolution, spatial frequency giving 10% maximal response.

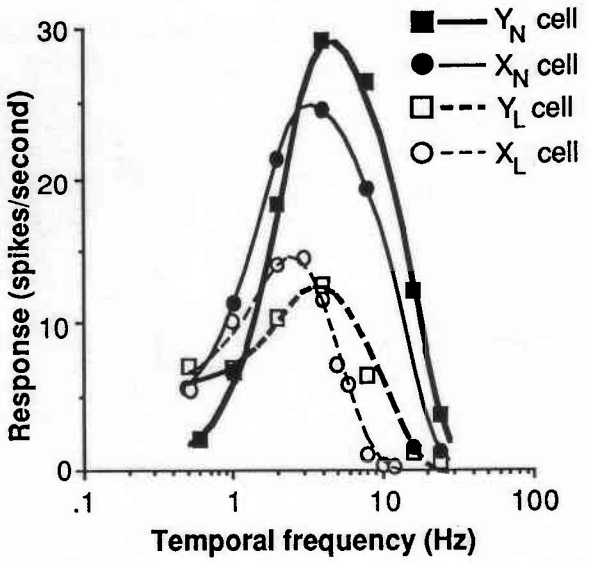

FIG. 3. Temporal frequency tuning curves for 4 geniculate cells are shown. Stimulus was a sinusoidally modulated spot. First harmonic response amplitudes are plotted against temporal frequency, and best-fitting difference of gaussian curves through the points are shown. Optimal temporal frequencies and temporal resolutions for these 4 cells were 4.4 and 25 Hz for the Y_N-cell, 3.3 and 22 Hz for the X_N-cell, 3.6 and 14 Hz for the Y_L-cell, and 2 and 9 Hz for the X_L-cell.

quency tuning. X_L-cells had slightly larger centers and smaller surrounds than X_N-cells but the differences were not significant in our small sample ($P > 0.05$, t test). These relationships held at all eccentricities. These results indicate that the differences between lagged and nonlagged X-cells have little to do with their spatial receptive-field properties.

Temporal responses

The temporal response properties of geniculate cells were analyzed by modulating stimulus luminance sinusoidally at various temporal frequencies. This provided two kinds of information for each cell. First, the amplitude of the response as a function of temporal frequency gave a description of the cell's temporal tuning. Second, the phase of the response provided a description of the cell's response timing.

TUNING. We tested cells with both sinusoidally modulated spots and drifting gratings. The amplitude of the first harmonic component of the response (which dominated the responses of all cells) against temporal frequency was fit by a difference of gaussians function of four parameters. This is formally identical to the procedure used in the spatial domain, but here, the difference of gaussians does not represent an explicit receptive-field model. Instead it is simply a convenient way to estimate optimal temporal frequency, temporal resolution, peak amplitude, and tuning widths. Figure 3 shows tuning curves for four representative cells. All cells had band-pass tuning. We saw no clear examples of low-pass tuning. All cells responded well at temporal frequencies between ~1 and 3 Hz but varied widely in their responses to higher frequencies. The X_L-cell illustrated in Fig. 3 peaked at 2 Hz and failed to respond beyond ~9 Hz. The Y_L-cell responded somewhat better to high frequencies. The two nonlagged cells discharged more vigorously at all frequencies above 2 Hz, continuing to fire out to ~20 Hz.

Figure 4 shows the distribution of preferred temporal frequencies to sinusoidally modulated spots for each group of cells. The average values for this and other temporal response measures are summarized in Table 2. Comparing X- and Y-cells, it is clear that there is a substantial range of optimal frequencies within each class and overlap between classes. The mean optimal temporal frequency for Y_N-cells is only slightly higher than for X_N-cells when tested with spots ($t = 1.4$, $P = 0.08$). Comparing lagged and nonlagged cells, there is also a sizable range within and overlap between the groups, but X_L-cells preferred much slower stimuli than X_N-cells ($t = 3.7$, $P < 0.001$). No X_L-cells had optimal temporal frequency above 3.4 Hz. X_N-cells were heterogeneous in their temporal tuning, ranging from units that preferred frequencies under 1 Hz up to cells with the highest optimal frequencies found. Y-cells were more tightly grouped around their mean. Y_N- and Y_L-cells had similar temporal frequency preferences ($t = 0.2$, $P = 0.42$).

Temporal resolution was taken as the frequency above the optimum that would give a response of 10% of the peak amplitude. No difference in mean temporal resolution was observed between X- and Y-cells when tested with either spots or gratings (Table 2). However, lagged and nonlagged cells differed significantly on this measure ($t = 3.8$, $P <$

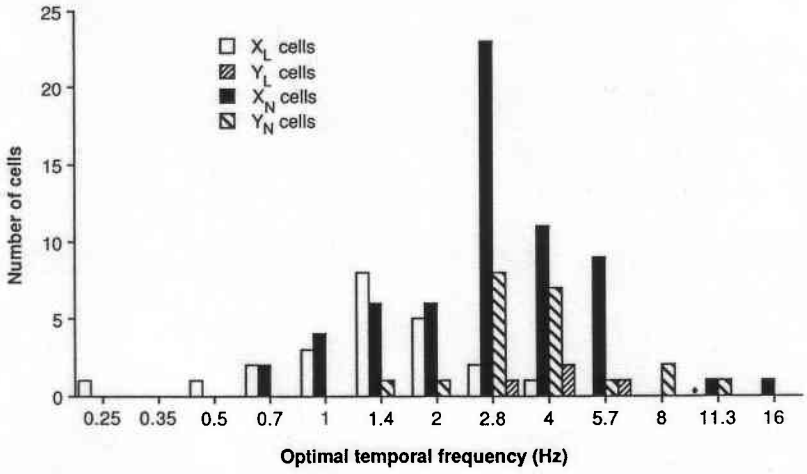

FIG. 4. Distribution of optimal temporal frequency when tested with sinusoidally modulated spots is shown for each group of cells. Included are 24 X_L-cells, 4 Y_L-cells, 63 X_N-cells, and 21 Y_N-cells. No cell was low-pass, but a few X-cells had very low preferred frequencies. X-cells were distributed more broadly than Y-cells, which clustered around 4 Hz. Eighty-nine percent of the cells had optimal temporal frequencies between 1 and 8 Hz.

TABLE 2. *Temporal response properties*

Cell Type	Phase Latency, ms	φ_0, cycles	Spot ω_{opt}, Hz	Spot Resn, Hz	Spot Amp, imp/s	Grating ω_{opt}, Hz	Grating Resn, Hz	Grating Amp, imp/s
X_L								
Mean ± SE	133 ± 4 (33)	0.096 ± 0.15 (33)	1.5 ± 0.2 (24)	9 ± 1 (24)	19 ± 2 (24)	3.13 ± 0.9 (9)	17 ± 4 (9)	14 ± 1 (9)
Range	94 to 197	−0.08 to 0.30	0.3 to 3.4	3 to 23	6 to 38	0.7 to 9.6	3 to 31	9 to 19
X_N								
Mean ± SE	63 ± 2 (77)	−0.116 ± 0.007 (76)	3.4 ± 0.3 (63)	22 ± 2 (63)	42 ± 3 (63)	4.7 ± 0.8 (18)	25 ± 4 (18)	33 ± 5 (18)
Range	37 to 107	−0.26 to −0.02	0.8 to 13.8	7 to 73	11 to 107	0.1 to 14	8 to 54	10 to 75
Y_L								
Mean ± SE	130 ± 14 (4)	−0.004 ± 0.023 (4)	4.3 ± 0.6 (4)	13 ± 1 (4)	27 ± 7 (4)	4.7 ± 1.1 (4)	18 ± 3 (4)	31 ± 7 (3)
Range	109 to 170	−0.07 to 0.03	3.2 to 6.1	11 to 15	12 to 44	2.0 to 6.9	10 to 22	18 to 38
Y_N								
Mean ± SE	59 ± 2 (30)	−0.180 ± 0.010 (27)	4.1 ± 0.5 (21)	22 ± 1 (21)	41 ± 4 (21)	6.0 ± 0.7 (10)	26 ± 5 (10)	35 ± 7 (10)
Range	35 to 91	−0.3 to −0.1	1.6 to 11.4	15 to 38	7 to 85	3.1 to 10.8	10 to 61	3 to 83

Number of cells tested in parentheses. φ_0, absolute phase; ω_{opt}, optimal temporal frequency; resn, temporal frequency giving 10% maximal response; Amp, maximal response amplitude.

0.001 for X-cells; $t = 3.2$, $P < 0.005$ for Y-cells). Among individual groups, X_L-cells had the poorest resolution; a number of them ceased firing to spot modulation rates above 4 Hz. Only 25% (6 out of 24) of the X_L-cells had resolutions above 10 Hz compared with 85% of the X_N-cells. Y_L-cells, despite having relatively high optimal temporal frequencies, did not respond well to frequencies above 10 Hz; their temporal resolution ranged from 11 to 15 Hz when tested with spots. We should note that all cells responded relatively better to gratings than to spots at higher temporal frequencies, although the spot stimuli generated stronger maximal response amplitudes. Nevertheless, the relationships among the four cell groups were similar when tested with either stimulus.

Taken together, these data reveal that differences in temporal tuning that exist among geniculate cells are more associated with the lagged/nonlagged dichotomy than with the X/Y distinction. The main difference between lagged and nonlagged cells is the poorer resolution of the former. These differences are clearly important yet do not account for the differences in the response profiles of lagged and nonlagged cells when tested with the four-part flashing spot stimulus (Figs. 1 and 2). Considerable overlap was observed in all of our measures of tuning. We only observed a clear separation in the temporal responses of lagged and nonlagged cells when we analyzed the timing, or phase, of the responses.

TIMING. The sinusoidally modulated spot experiments permitted the systematic extraction of information about the timing of cells' responses. Figure 5 illustrates typical responses from three cells: ON-center X_N- and X_L-cells and an OFF-center X_N-cell. The spot luminance was modulated at 1 Hz, as shown at the *bottom* of the figure. The ON-center cells fire when the stimulus is bright. The nonlagged cell begins to fire just after the spot reaches its darkest point (at 0.75 s) and the luminance begins to increase. Peak firing occurs just before the peak of the stimulus luminance (at 0.25 s). The activity declines rapidly as the spot darkens. In contrast, the lagged cell begins to respond as the spot reaches its brightest point, and most of its firing occurs as the luminance decreases. Nonetheless, the lagged cell differs from the OFF-center cell, whose firing clearly peaks just before the luminance trough (at 0.75 s). By this point the X_L-cell has nearly ceased firing. At low temporal frequencies lagged cells discharged at a time partway between the firing of ON- and OFF-center nonlagged cells.

We quantified these differences in response timing by measuring the first harmonic *response phase* relative to the stimulus. If a cell responded in synchrony with the stimulus, reaching its peak firing when the spot was brightest, the response phase was taken to be zero cycles. If response peaked when the spot reached its darkest point, phase would be 0.5 cycles. As a normalization, however, we sub-

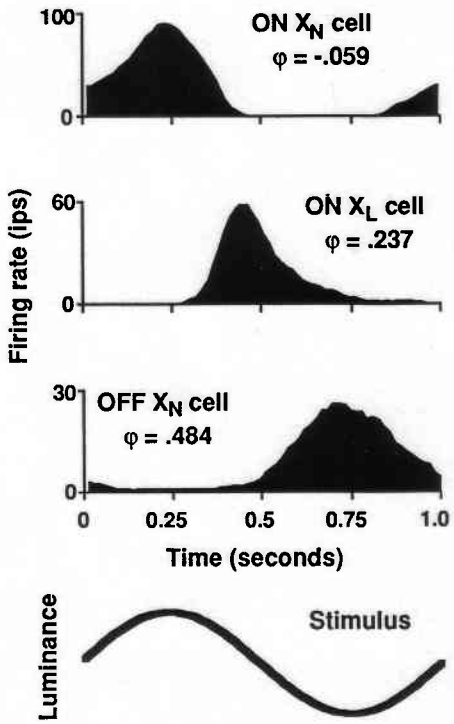

FIG. 5. Response histograms to sinusoidally modulated spot stimuli are shown for 3 different cell types. Stimulus in all 3 cases was modulated at 1 Hz. Responses occurred at different times for these 3 cells. First harmonic response phase is given for each cell, with larger values of phase corresponding to responses that occurred later in the stimulus cycle as shown.

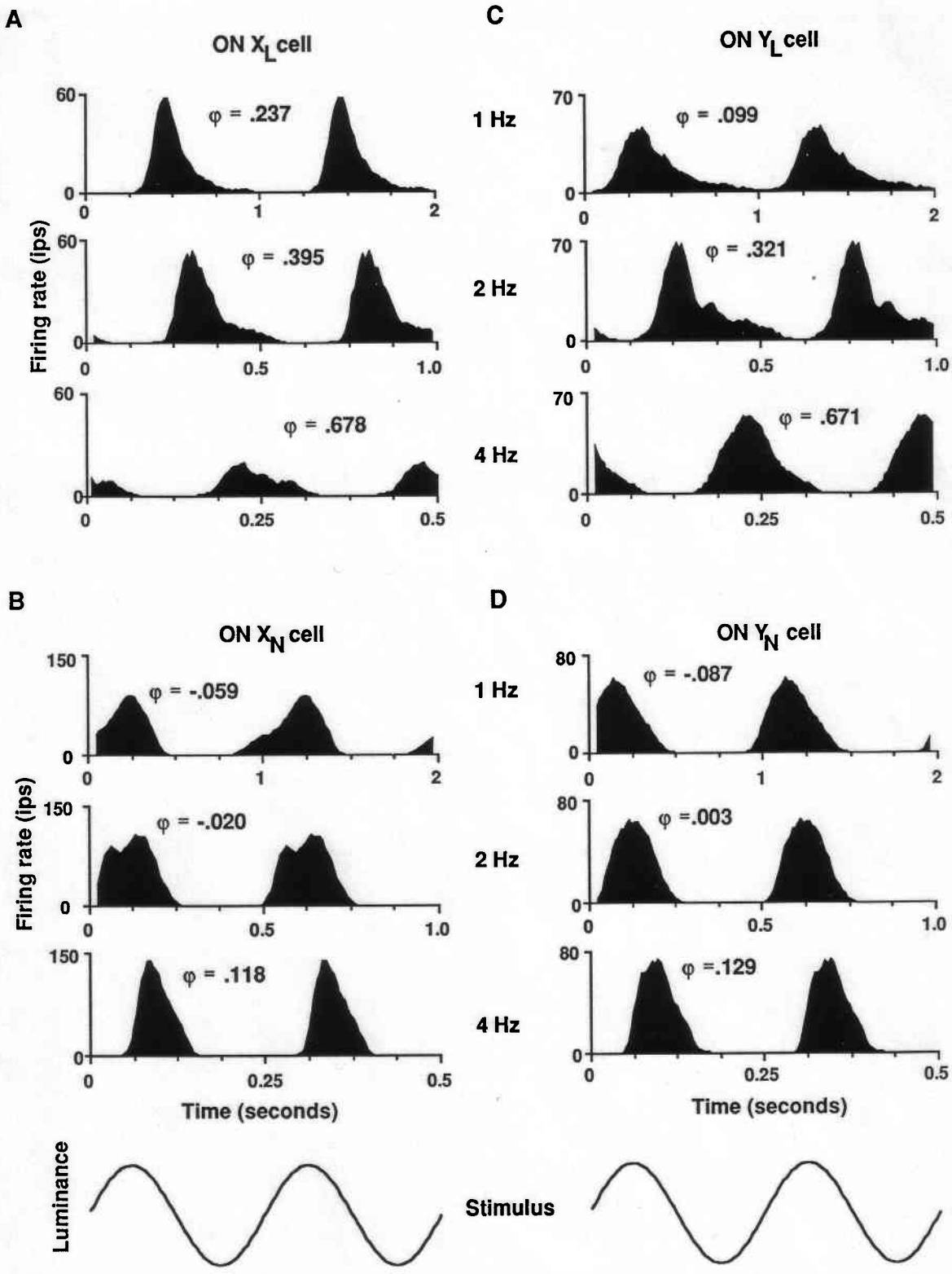

FIG. 6. Peristimulus time histograms of the responses of 4 different cell types to small spots sinusoidally modulated at 3 temporal frequencies. Two cycles are shown for clarity. First harmonic response phase is shown above each histogram. For each cell, response phase increases with frequency. This increase, which corresponds to a visual latency, is greatest in the lagged cells (*A* and *C*). Lagged cells show phase lags at 1 Hz relative to the nonlagged cells (*B* and *D*) of about one-quarter cycle.

tracted 0.5 cycles from phase values for OFF-center cells. At low temporal frequencies, response phase was assigned to the interval from −0.25 to 0.25 cycles. Responses that occurred later in the stimulus cycle were assigned larger phase values; this convention means that response phase is a measure of phase lag (Lee et al. 1981). The phase of the ON-center X_N-cell response in Fig. 5 is −0.059 cycles, whereas the lagged-cell response phase is 0.237 cycles, and the OFF-center X_N response phase is 0.484, which became −0.016 after normalization.

Physiologically, response phase is determined by two factors. The first is where in the stimulus cycle the excitation arises, for instance whether the cell is excited by increasing luminance, peak brightness, decreasing luminance, or peak darkness. The second factor is the delay that intervenes between the stimulus events and the cell's response to these events, that is, the latency of the evoked response. These two factors are confused in the response to a single temporal frequency. The late response of the lagged cell could be due to either a tendency to fire late in the stimulus cycle, or to a long latency, or to both factors.

The intrinsic phase can be distinguished from the effects of latency, however, by obtaining phase values at more than one temporal frequency. A pure delay adds a phase lag that is proportional to the frequency. Latency, which includes pure delays and integration time associated with temporal filtering, becomes the slope of the phase versus frequency plot. The intrinsic response phase corresponds to the phase that would be seen in the absence of latency effects, which is the phase at 0 Hz, because at 0 Hz latency adds no phase lag (cf. Lee et al. 1981).

To dissociate the effects of latency and intrinsic phase, we therefore tested each cell at a range of temporal frequencies. Figure 6 illustrates how response timing changes with temporal frequency. Responses to spots modulated at 1, 2, and 4 Hz are shown for four representative cells. Two cycles are shown here for clarity. As temporal frequency increases, the responses occur later in the stimulus cycle. The response phase of the X_L-cell in Fig. 6*A* increases from 0.24 cycles at 1 Hz to 0.40 cycles at 2 Hz to 0.68 cycles at 4 Hz. The cells in *B–D* behave similarly, but the rate of change is slower in the nonlagged cells than in the lagged cells. In addition to this difference in latencies (i.e., the rate of change of phase with temporal frequency) between the lagged and nonlagged cells, there is a clear difference in the phase at 1 Hz. Even at low temporal frequencies, lagged cells respond later in the stimulus cycle than do nonlagged cells. This suggests a difference in the intrinsic phase. Testing cells at several temporal frequencies thus revealed differences in both latency and intrinsic phase.

We plotted response phase against frequency for four representative ON-center cells in Fig. 7. Measured phase values were extremely reliable when an adequate response was present, with SDs of ~0.005 cycles over ten measurements at 4 Hz; this is on the order of the binwidth. Phase increased approximately linearly with frequency, with a consistent trend toward convexity. That is, the slope decreased slightly with frequency in most cells; all cell types showed this tendency. At low temporal frequencies (~0.5 Hz) phase was often advanced. Higher frequencies could also lead to apparent phase advances. However, these points were also associated with low response amplitudes and less reliable phase values. Linear regressions were computed across temporal frequencies where the cell responded adequately (usually 1–8 Hz), with regression coefficients of at least 0.98 and generally above 0.99. Because the phase data are well approximated with straight lines, we will describe response phase in terms of two numbers, the slope and the intercept. The slope of the regression line will be referred to as *latency*; the phase intercept will be referred to as intrinsic or *absolute phase.*

The slopes of the phase versus frequency data in Fig. 7 show that the lagged cells (open symbols) have longer latencies than the nonlagged cells (filled symbols). Table 2 includes mean latencies for each cell type. X- and Y-cells differed little in this measure. Lagged-cell latencies averaged 70 ms longer than nonlagged cell values. Lee et al. (1981) found geniculate latencies of 35–42 ms using similar methods but with much brighter stimuli. Based on the response-phase values of their cells, all appear to have been nonlagged (see below).

The latency calculated from the slope of the phase versus frequency data was compared with the half-rise latency obtained from the response to the flashing spot stimulus. These two measures of latency are reasonably well correlated across the X_N-cells ($r = 0.52$, $P < .0001$, $n = 77$) but not across either X_L-cells ($r = 0.012$, $n = 33$) or Y_N-cells ($r = 0.348$, $P < 0.05$, $n = 29$). For Y_N-cells, the limited range of half-rise latencies (Fig. 2) provides too little variance to allow any correlation to show up. For X_L-cells the lack of correlation is due to the often extended inhibitory dip seen in the flash histograms, which can make half-rise latencies as long as 750 ms. We discuss below how these measures of latency are related.

We next consider the parameter of absolute phase. The data in Fig. 7 intersect the ordinate at different points. The nonlagged cells have absolute phase values below zero, be-

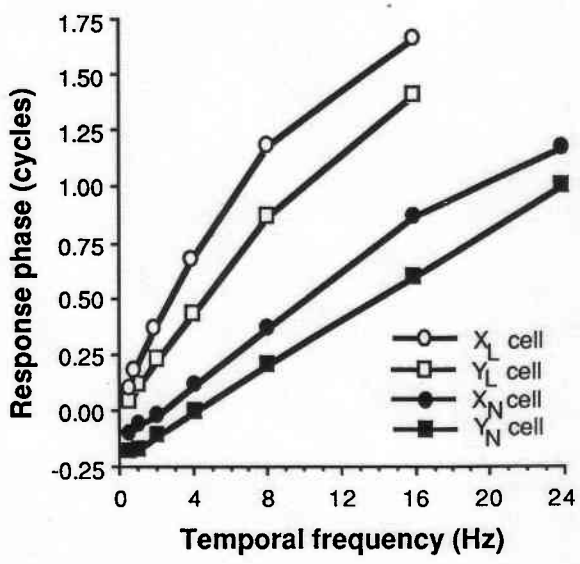

FIG. 7. Response phase is plotted against temporal frequency for 4 cells. Phase increases approximately linearly with frequency. Slope (latency) and intercept (absolute phase) for these cells were 150 ms and 0.064 for the X_L-cell, 109 ms and 0.003 for the Y_L-cell, 57 ms and −0.111 for the X_N-cell, and 51 ms and −0.206 for the Y_N-cell.

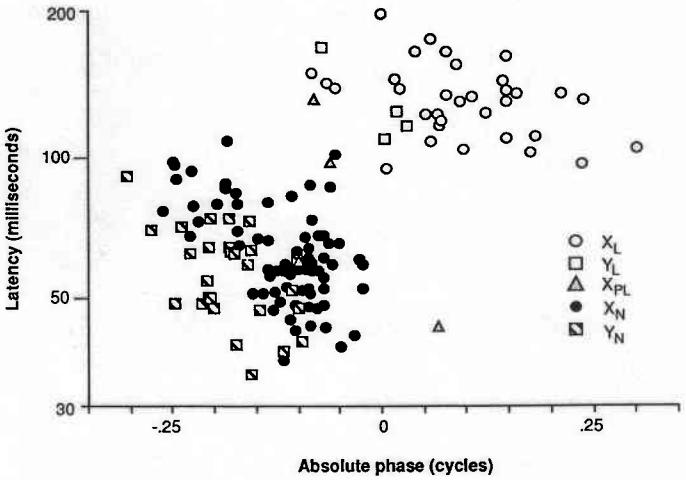

FIG. 8. Latency and absolute phase values derived from the response phase vs. temporal frequency plots are shown for each cell group. As in Fig. 2, open symbols represent lagged cells; filled symbols represent nonlagged cells.

cause they respond in advance of the stimulus, as seen in the histograms of Fig. 6. The X_L-cell lags the stimulus, on the other hand. The Y_L-cell has intermediate behavior, responding approximately in phase with the stimulus but with a long latency. Mean values for absolute phase are given in Table 2. Y_N-cells had the earliest absolute phase values followed by X_N-cells, Y_L-cells, and X_L-cells. The difference between any two of these means is statistically significant ($P < 0.001$). Thus the late responses of lagged cells are not entirely due to their longer latencies but depend on the linkage of the response to the offset of the stimulus (i.e., the portion of the stimulus cycle after the appropriate contrast has peaked) rather than the onset. The half-rise latency in X_L-cells, which we noted above was uncorrelated with the phase latency, is correlated with absolute phase ($r = 0.516$, $P < 0.001$, $n = 33$), suggesting that the absolute phase difference might characterize the difference between lagged and nonlagged cells.

Lagged cells are indeed distinguished from nonlagged cells by the two parameters derived from the response-phase data. Figure 8 shows the results from all cells as a scatterplot of latency versus absolute phase. Almost no overlap exists between the distributions of lagged and nonlagged cells in this plane. Three X_{PL}-cells (triangles) and one X_N-cell had borderline values. A fourth X_{PL}-cell gave phase values indistinguishable from X_N data (hidden amongst filled circles); this cell had the shortest half-rise and half-fall latencies of the four X_{PL}-cells (Fig. 2). The Y_L-cells had long latencies and absolute phase values near zero. The distributions of Y-cells are shifted toward earlier phase values and shorter latencies compared with the X-cell distributions, but overlap.

The separation achieved by joint consideration of these two parameters can also be seen in Fig. 9, where the response phase at 1 Hz is plotted for each cell group. Practically every cell responded well at 1 Hz, making it a suitable frequency for comparisons. The phase at 1 Hz is the sum of the phase at 0 Hz (in cycles) and the latency (in seconds). Lagged and nonlagged cells have nonoverlapping distributions. At 1 Hz, the response phase difference between X_L- and X_N-cells, or between Y_L- and Y_N-cells, is about a quarter cycle.

Because of the latency difference, the response phase difference between lagged and nonlagged cells increases with frequency. Figure 10 shows the average phase versus frequency regression lines for each cell group. The quarter-cycle phase difference at 1 Hz increases to about a half cycle by 4 Hz and is even greater at higher temporal frequencies. Note that we have only plotted phase values for temporal frequencies up to 16 Hz for lagged and partially lagged cells, because very few responded beyond that point.

COMPARISON OF FREQUENCY AND TIME DOMAINS. We have seen that lagged and nonlagged cells can be distinguished in two ways, either by measuring response latencies to onset and offset of a square-wave-modulated flashing spot or by measuring response phase to a sinusoidally modulated spot. We now show how these two analyses are related by translating the frequency domain data back to the time domain. To the extent that cells respond linearly in time, the results from the sinusoidally modulated-spot experiments provide a description of the response to an arbitrary stimulus. We found that key features of the responses to the flashed stimulus were predicted under simple linear assumptions, as will be shown below. By describing the dynamics of these cells we take a step toward understanding the mechanisms underlying their responses.

The frequency domain response of each cell was modeled by the difference of gaussians function that best fit the amplitude data multiplied by the phase values derived

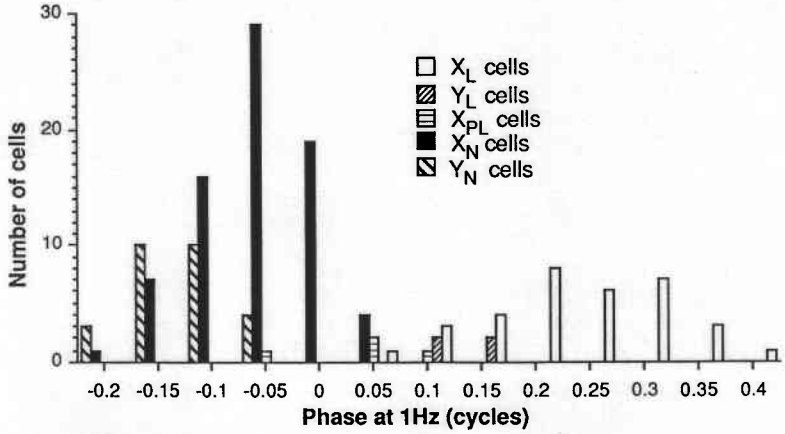

FIG. 9. Distribution of response phase values obtained at a temporal frequency of 1 Hz is shown for each group of cells. OFF-center cells have been shifted by a half-cycle and pooled with ON-center cells. Distributions of lagged and nonlagged cells have no overlap at 1 Hz (or at higher frequencies). Thus cells can be identified as lagged or nonlagged by simply measuring the response phase at 1 Hz.

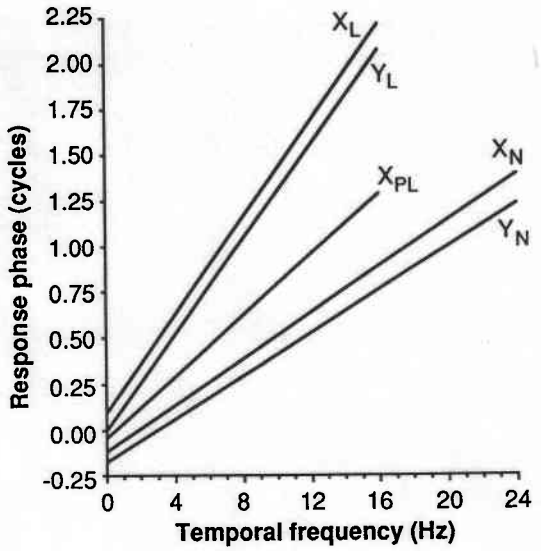

FIG. 10. Phase vs. temporal frequency relationships are summarized for each type of cell. Lines are drawn with slope corresponding to the average latency and intercepts corresponding to the average absolute phase (see Table 2 for values). Lagged and nonlagged cells are distinct, but X- and Y-cells of the same type have similar response phase behavior. X_{PL}-cells fall in the middle. Variation across the population would fill up the entire phase vs. frequency plane. Difference between lagged and nonlagged cell phase values amounts to ~0.25 cycles at low temporal frequencies, but expands to ~0.5 cycles by 4 Hz.

from the linear regression fit. This model has deficiencies, particularly at low temporal frequencies, but is not critical for the main points below. An array of complex numbers was thus generated (for frequencies between −32 and 32 Hz), which was used to derive a real-valued function of time via a FFT routine (Press et al. 1986). This *impulse response function* represents the theoretical response of the cell to an infinitely intense stimulus of the appropriate contrast for the cell's center sign flashed in the receptive field infinitely briefly. More formally, the impulse has a fixed area but vanishing duration. By convolving the impulse response function with any stimulus, the response to that stimulus is obtained, given linear temporal summation. The impulse response function provides a complete description of the dynamics of a linear system.

Figure 11 illustrates four examples of impulse response functions obtained in this way. The four-part flashing spot histogram is shown along with each impulse response for comparison. The X_N-cell in Fig. 11*A* gave very phasic responses with no sustained component. The impulse response for this cell (Fig. 11*B*) shows an excitatory response for the first 78 ms followed by a strong inhibition for the next 188 ms. Figure 11*G* shows a strongly lagged X-cell with a strong inhibitory dip and anomalous offset discharge. The cell's impulse response (Fig. 11*H*) shows a short latency inhibition lasting 109 ms followed by 219 ms of excitation. Between these extremes lie the X_N- and X_L-cells in *C* and *E*. In Fig. 11*D*, the impulse response for the X_N-cell is dominated by excitation with a weak but long-lasting secondary inhibition. This cell had a strong sustained component in its flash response (Fig. 11*C*). The X_L-cell in Fig. 11*E* has only a brief early inhibitory phase in its impulse response (Fig. 11*F*) matching the brief inhibitory dip in the flash response.

The difference in absolute phase (φ_0) between lagged and nonlagged cells determines the initial phase of the impulse response function: initial excitation for nonlagged cells whose absolute phase is less than zero and initial inhibition for lagged cells whose absolute phase is greater than zero.[1] The early inhibition in lagged cells is one key attribute of their response to flashing spots; the other key attribute is the anomalous offset discharge. The responses to sinusoidally modulated stimuli predict the existence of the anomalous offset discharge to flashing spots. At stimulus offset the early inhibition is removed, whereas the slower excitatory response remains. We analyze this phenomenon more fully below. Both the anomalous offset discharge and the inhibitory dip are related to the absolute phase lagging the stimulus.

Figure 11 also illustrates that the more transient nonlagged cells (e.g., Fig. 11*A*) have stronger secondary inhibition (Fig. 11*B*). This inhibition cancels the earlier excitation, suppressing activity after a certain time. The absolute phase in these transient cells leads the stimulus by nearly a quarter cycle. Similarly, a strongly lagged cell like the one in Fig. 11*G* has strong early inhibition, which is only overcome by a late excitatory phase (Fig. 11*H*). The absolute phase in these cells lags the stimulus by nearly a quarter cycle.

The impulse response function is a general description of the time domain response of these cells but is not directly comparable with data because cells do not respond well to an impulse. For direct comparison, we simulated the responses to the four-part flashing spot stimulus with the use of actual data obtained from cells' responses to sinusoidally modulated stimuli. Figure 12 compares measured flash response histograms with curves generated from the simulations. Because the flashing spot stimulus has a discrete spectrum, these reconstructions were derived directly from the amplitude and phase data, by computing the sum

$$\text{Response}(t) = \sum (-1)^{[n/4]} \frac{A}{n} \cos \{2\pi[n\omega(t - L) - \varphi_0]\}$$

where the sum was taken over the first 26 odd harmonics, $n = 1, 3, 5, \ldots, 51$. A represents the response amplitude at the frequency $n\omega$, which is divided by n to approximate the decline in response with contrast, because the contrast of the stimulus component at the frequency $n\omega$ is $1/n$ times the contrast of the fundamental component at frequency ω. (Other choices for the amplitude dependence on contrast, including scaling by log contrast or using measured responses, did not greatly improve the results, so the simplest assumption was subsequently used.) L represents the latency and φ_0 the absolute phase. The roles of latency and absolute phase in determining the response waveform are explicit in this formulation: the latency simply shifts the whole response profile, whereas the absolute phase determines the phase of each component. It is important to note that all components of the square-wave stimulus have ris-

[1] Writing the response phase as $L\omega + \varphi_0$, where L is latency and φ_0 is absolute phase, the Fourier transform of the frequency-domain response becomes the Fourier transform of the amplitude tuning function with a time delay of L, multiplied by the absolute phase φ_0.

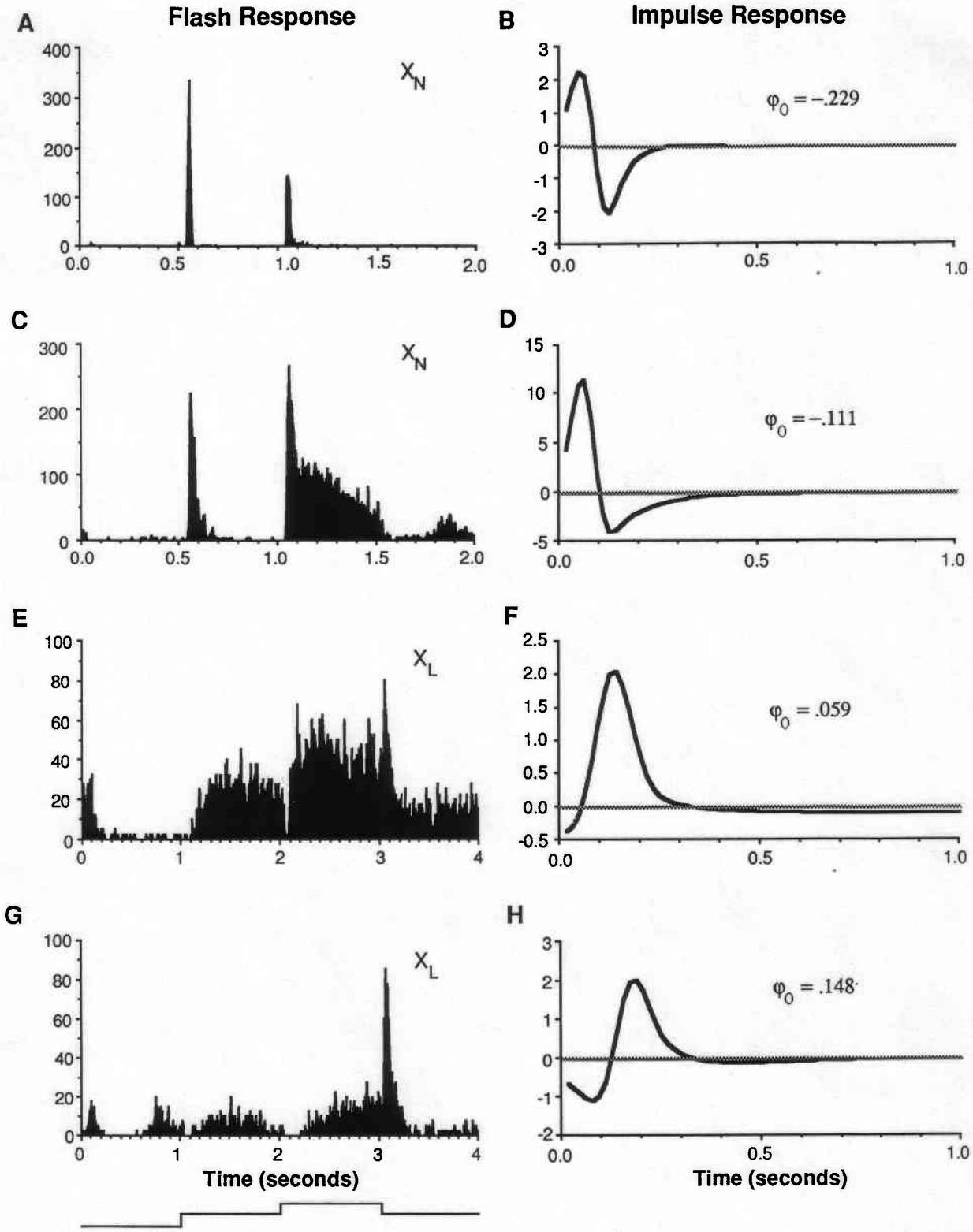

FIG. 11. Impulse response functions derived from the responses to sinusoidally modulated spots are compared with responses to the 4-part flashing spot stimulus for 4 X-cells. These cells range from a very transient nonlagged cell (*A* and *B*) to a nonlagged cell with some sustained response (*C* and *D*) to a lagged cell with only a brief inhibitory dip and small anomalous offset discharge (*E* and *F*) to a very lagged cell with a prolonged inhibitory dip and a strong anomalous offset discharge (*G* and *H*). Absolute phase values range from almost a quarter-cycle phase lead to a phase lag of more than an eighth of a cycle. One of the effects of these phase values on impulse response functions is to determine whether the initial response is excitatory (*B* and *D*) or inhibitory (*F* and *H*). Scales for the flash response histograms are in spikes/s. Scale for the impulse response functions is arbitrary. Step size in impulse response functions is ~16 ms based on extrapolation of the frequency response to 32 Hz.

ing edges where their sum (the square wave) has rising edges, and the same holds for the falling edges. When absolute phase is <0, the response components pile up at the rising edges of the stimulus giving a transient excitatory response (Fig. 12*A*). When absolute phase is between 0 and 0.25, as it is for ON-center X_L-cells (Fig. 8), the response components pile up at the falling edges instead, providing the anomalous offset discharge (Fig. 12*B*). The match between the curves and the histograms is inaccurate as far as amplitude is concerned, but the match to the timing of presumptive inhibitory and excitatory responses is excellent. The key features of the flash responses were consistently reproduced by these linear approximations derived from the phase data.

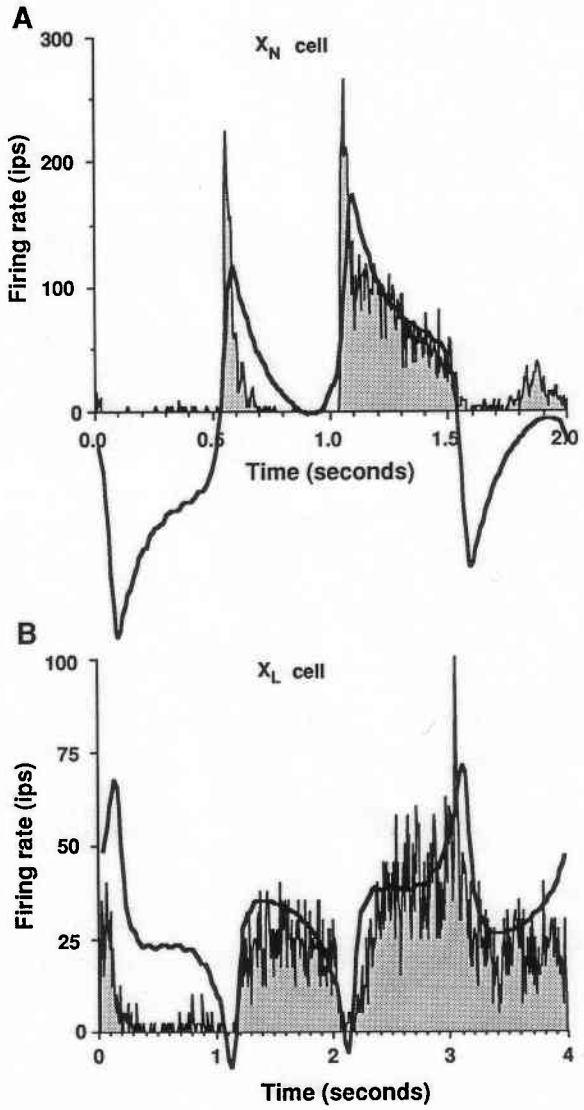

FIG. 12. Responses to the 4-part flashing spot stimulus are compared with predictions derived from responses to sinusoidally modulated spots. Solid lines show the sums of 26 sine waves having amplitudes, frequencies, and phases corresponding to responses to sine-wave components of the 4-part stimulus. Vertical scaling of solid curves is arbitrary, and they have been placed by eye to match sustained portions of responses. *A*: transient responses to luminance increases are matched in this nonlagged X-cell. Reconstruction is more sustained during the background step preceding the bright step. Discharges during the background step after the bright step match the increase in the reconstruction. *B*: the inhibitory dip and anomalous offset discharge of this lagged X-cell are present in the reconstruction. Other features of the response profile also correspond to features in the reconstruction.

Although linear temporal summation allows a useful approximation of responses to complex stimuli in terms of responses to simpler stimuli, our cells behave nonlinearly in several important ways. The response to a sinusoidal stimulus is usually somewhat rectified (Fig. 6) and contains other distortions that we have ignored for simplicity (all cells were dominated by the first harmonic response, however). Furthermore, response is not linear with stimulus contrast, as we discuss further below. The dependence of the response to a complex stimulus on subthreshold summation is also unclear. Strictly linear predictions therefore fail quantitatively. Nevertheless, appeals to nonlinear mechanisms are unnecessary to account for phenomena such as the inhibitory dip and anomalous offset discharge in lagged cells and the transient firing pattern seen in most cells. The time when spikes occur during stimulus presentation matches the linear prediction from the frequency domain, *if response phase is taken into account.*

Contrast

Given the differences between lagged and nonlagged cells in temporal response properties but similarities in the spatial domain, we were interested in how the cells compared in the contrast domain. We tested 58 cells with drifting gratings of optimal temporal and spatial frequencies, varying the contrast over a range from 0.0025 to 0.96. The first harmonic component of the response was plotted against log contrast, and the amplitude was fit with a function that was constant up to a threshold, then increased linearly with log contrast. This function had three parameters (Fig. 13, *top plot* for each cell): the constant (the noise level), the threshold, and the slope of the increasing piece, which is a measure of contrast gain. The phase data for those points above threshold were fit with a line (phase vs. log contrast) so that the slope could provide a measure of phase advance with contrast (Fig. 13, *bottom plot* for each cell). This method gave threshold values that were consistent with our subjective estimates of threshold. The data were well fit by the piecewise linear functions. This method makes contrast threshold independent of contrast gain, unlike methods dependent on criterion response levels (Enroth-Cugell and Robson 1966). Subjective estimates of threshold likewise rely on judging whether responses surpass some criterion. Threshold, gain, and phase advance measurements are summarized in Table 3.

THRESHOLD AND GAIN. Contrast thresholds did not differ significantly between cell types (Table 3; $P > 0.15$ for all comparisons). X_L-cells often appeared to have relatively high thresholds because they were difficult to drive. The nonlagged cells in Fig. 13, *A* and *C*, were clearly driven above contrasts of 0.02, whereas the X_L-cell in *B* was difficult to drive at contrasts below 0.1. The objectively determined thresholds of these cells differed little, however. The relative ease of driving nonlagged cells appears to depend more on their larger contrast gain than on lower thresholds. Lagged and nonlagged X-cells differed significantly ($P < 0.001$) in contrast gain, which increased from 5.3 in X_L-

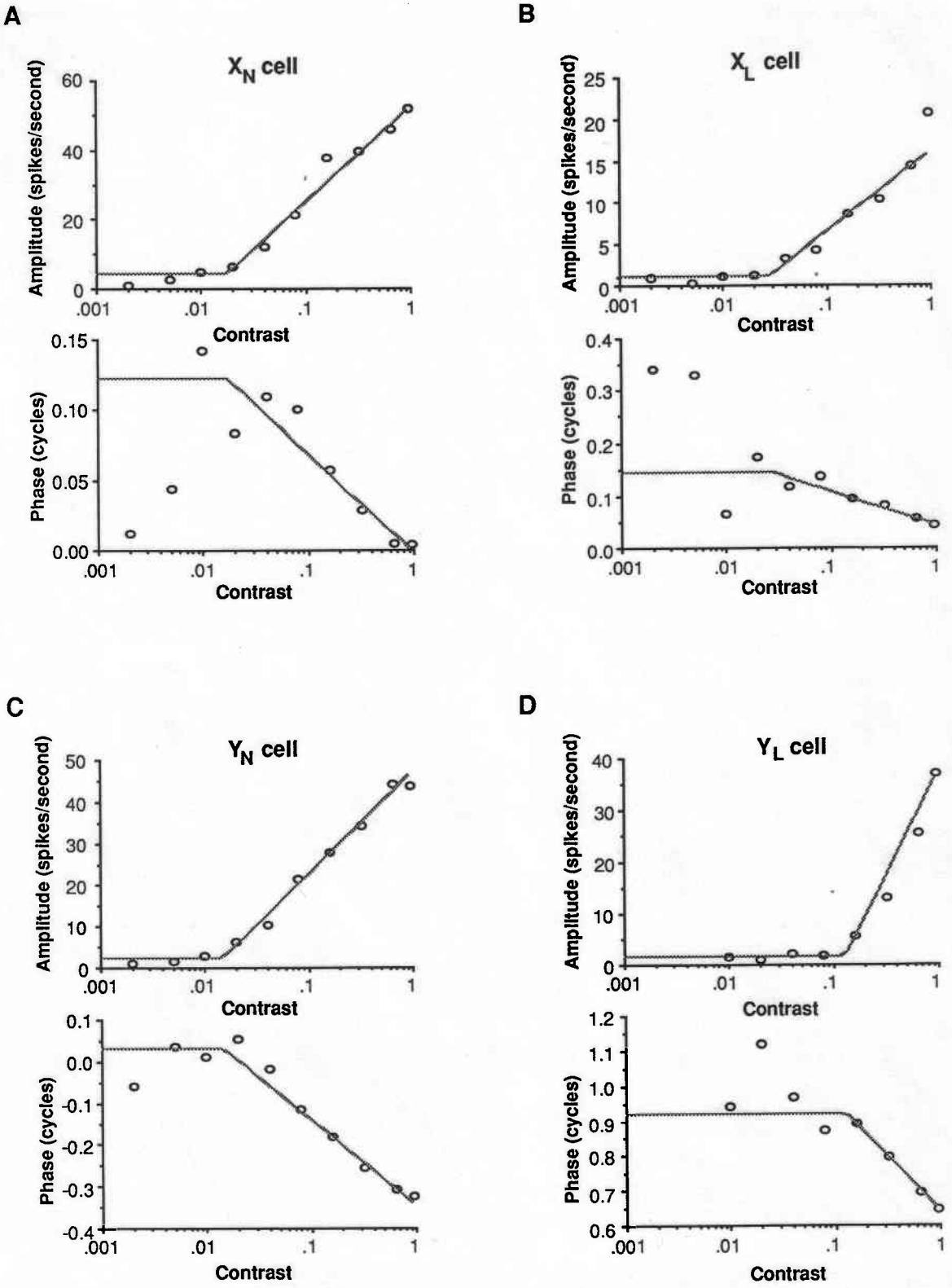

FIG. 13. Contrast-response functions are shown for 4 cells. Amplitude (*top*) and phase (*bottom*) are plotted against log contrast. Data were fit by functions that were constant up to a threshold and linear beyond it. These fits yielded 5 parameters: subthreshold amplitude and phase, threshold, contrast gain, and phase advance. Cells were tested with gratings of optimal spatial and temporal frequencies: *A*, 6 Hz and 1.0 cpd; *B*, 2 Hz and 0.4 cpd; *C*, 4 Hz and 0.125 cpd; *D*, 4 Hz and 0.125 cpd. Thresholds, gains (in spikes/s-octave), and phase advances (in cycles/octave) were *A*, 0.02, 8, 0.02; *B*, 0.03, 3, 0.02; *C*, 0.02, 7, 0.06; *D*, 0.13, 12, 0.10.

TABLE 3. *Contrast response parameters*

Cell Type	Threshold	Gain, imp·s^{-1}·octave^{-1}	Phase Advance, cycles/octave
X_L			
Mean ± SE	0.056 ± 0.016 (14)	5.3 ± 0.6 (14)	0.013 ± 0.005 (11)
Range	0.013–0.235	1.12–8.39	−0.02–0.028
X_N			
Mean ± SE	0.056 ± 0.016 (29)	9.6 ± 1.0 (29)	0.023 ± 0.003 (19)
Range	0.013–0.433	2.40–26.37	0.0025–0.058
Y_L			
Mean ± SE	0.096 ± 0.06 (4)	14.0 ± 8.4 (4)	0.071 ± 0.036 (4)
Range	0.007–0.266	2.8–38.4	−0.011–0.157
Y_N			
Mean ± SE	0.061 ± 0.02 (11)	13.0 ± 2.4 (11)	0.059 ± 0.005 (8)
Range	0.013–0.219	5.59–42.48	0.041–0.074

Number of cells tested in parentheses.

cells to 9.6 in X_N-cells to 13.0 in Y_N-cells, in units of spikes per second per octave of contrast. The four Y_L-cells tested varied widely in their contrast-response functions. The cell illustrated in *D* had a high threshold and gain, but another Y_L-cell had a low threshold (0.007) and low gain (4.0). Although the contrast response measurements from four Y_L-cells are inconclusive, the low response amplitudes obtained from Y_L-cells on other tests suggest that they share the weak contrast gain characteristic with X_L-cells.

PHASE ADVANCE. As contrast increases, some cells fire earlier or more transiently. One way to measure this change is to plot response phase against contrast (Fig. 13). As seen in these four typical examples, phase advances linearly with log contrast once threshold is exceeded. The X-cells both showed phase advances of 0.02 cycles/octave, whereas the Y_N- and Y_L-cells had phase advances of 0.06 and 0.09 cycles/octave, respectively. Shapley and Victor (1981) argued that the temporal transfer functions of cat *retinal ganglion cells* become more high pass with increasing contrast and referred to this effect as the contrast gain control. They showed phase advances of ~0.02 cycles/octave for X-cells and ~0.05 cycles/octave for Y-cells, when tested at 8 Hz and at low contrasts (Shapley and Victor 1978). We found similar average values (Table 3). The temporal frequency in our experiments was optimal, usually ~3 Hz. In a few runs we varied both contrast and temporal frequency and confirmed Shapley and Victor's results indicating that these effects were related to temporal frequency, with phase advances only appearing at higher frequencies. More extensive testing of X_L-cells at high frequencies might reveal larger phase advances. Unfortunately, X_L-cells respond poorly to high frequencies. Because the X_N- and Y_N-cells were tested at similar frequencies (e.g., Fig. 13, *A* and *C*), the weaker phase advances seen in X-cells were not entirely the result of the effect of temporal frequency.

Thus among X- or Y-cells there was little difference in the effects of contrast on lagged and nonlagged cells. Between X- and Y-cells there were significant differences, which reflect their retinal inputs (Shapley and Victor 1978). These data indicate that the geniculate mechanisms associated with the lagged/nonlagged dichotomy are not concerned with contrast-response processes, apart from reducing contrast gain in lagged cells.

DISCUSSION

Distinctions between cell groups

X- AND Y-CELLS. Our results are in agreement with previous reports that, as major classes, X- and Y-cells are readily distinguished by their spatial properties, including linearity or nonlinearity of spatial summation, receptive field–center size, and spatial frequency tuning (for review, see Sherman 1985). In comparison, we found only small differences between X- and Y-cells in temporal properties. Optimal temporal frequency was slightly higher in Y-cells on average, but temporal resolution was similar for the two functional classes. Response phase was advanced in Y-cells relative to X-cells on average, corresponding to more transient response profiles when tested with flashing spots. However, X- and Y-cells overlapped considerably on every measure of temporal response. These findings are in agreement with previous reports indicating that X- and Y-cells are much more similar in the temporal domain than in the spatial domain (Derrington and Fuchs 1979; Lehmkuhle et al. 1980; Sestokas and Lehmkuhle 1986; Sherman 1985). Moreover, they argue against the notion that the functional roles of Y- and X-cells are to subserve motion versus form perception, respectively (Blake and Camisa 1977; Ikeda and Wright 1972; Stone et al. 1979; Tolhurst 1973).

LAGGED AND NONLAGGED CELLS. Whereas the X/Y dichotomy does not reveal clear differences in temporal behavior among geniculate cells, the lagged/nonlagged dichotomy does. X_L-cells match X_N-cells in the spatial domain but give radically different responses in time. Similarly, Y_L-cells match Y_N-cells spatially but differ temporally. As a rough description, the X/Y distinction is spatial, and the lagged/nonlagged distinction is temporal. Furthermore, because the X/Y distinction is inherited from the retina (Cleland et al. 1971; Mastronarde 1987a) whereas the lagged/nonlagged distinction arises in the LGN, it appears that a major role of the LGN in visual information processing is to transform signals in the temporal domain.

Importance of phase differences in the LGN

RELATIONSHIP TO RESPONSE LATENCY. The differences in the temporal tuning properties of lagged and nonlagged cells are insufficient to account for the cells' markedly dif-

ferent response latencies to flashed spots (Fig. 1). For example, in simulations of time-domain data based on frequency-domain responses (e.g., Fig. 12), results were relatively insensitive to tuning parameters such as optimal temporal frequency. Rather than tuning, the temporal distinction between lagged and nonlagged cells depends on timing. The difference between lagged and nonlagged cells corresponded closely to the distinction between absolute phase values that lagged and that led the stimulus. All nonlagged cells had absolute phase leads, and all but a few lagged cells had absolute phase lags (Fig. 8 and Table 2). Absolute phase was the parameter that was correlated with the latency to the flashing spot in lagged cells.

RELATION TO DISCHARGE PATTERNS. The measures of response timing derived from responses to sinusoidal stimuli were surprisingly good at predicting patterns of cell discharge (i.e., the response profiles) to square-wave stimuli. That is, adding the first harmonic responses to each component of the four-part flashing spot stimulus produced good approximations to the actual responses to that stimulus (Fig. 12). These reconstructions were based on minimal assumptions, the main one being linear temporal summation, and relied critically on only the two parameters derived from the phase measurements. The most important parameter was the absolute phase, which predicted where response peaks and valleys would occur in the histograms. The latency parameter had a less obvious effect, usually shifting the histogram by <100 ms. The effects of the amplitude tuning curves on the response profile were restricted to determining the smoothness and the sharpness of the profile. The assumption that the response amplitude evoked by each component was proportional to its contrast was made for simplicity. The present data are insufficient to provide accurate estimates of the many additional parameters (related to distortion, subthreshold summation, rectification, and contrast dependence of both amplitude and phase) needed to obtain more accurate fits. Nevertheless, the simple model was successful at generating the distinctive features of the flash response histograms for practically all of the cells (numbering over 100) to which it has been applied. The success of this model implies that, to a large degree, the mechanisms generating lagged and nonlagged response profiles, as well as sustained and transient discharge patterns, act linearly in the temporal domain.

The fact that transient discharge patterns correspond to phase leads has not been appreciated by some authors. For example, Tolhurst et al. (1980) argued that temporal summation in visual cortical cells is nonlinear, based on comparing temporal tuning with the Fourier transformation of the derivative of transient responses to flashed stimuli. In discussing what sorts of nonlinearities might be involved, they speculated that the nonlinearity might be inherited from the geniculate, because geniculate neurons give similar transient responses. They ignored response phase, however, which we have shown produces appropriate impulse response functions and flash responses, without invoking strong nonlinearities. Although transient responses tend to be associated with higher temporal frequency tuning, it is the association with strong phase leads that determines the occurrence of a brief discharge at stimulus onset.

Mechanisms underlying X_L responses

The present investigation is descriptive but has implications for mechanisms. Lagged cell responses are characterized by an *absolute phase shift* and a *pure delay* or *latency increase* relative to nonlagged cell responses. Any proposed mechanism must account for these two timing changes.

The absolute phase shift in lagged cells is most simply accounted for by processes involving inhibition. In data from simultaneous recordings of retinal and geniculate neurons stimulated with flashing spots, Mastronarde (1987b) showed that lagged X-cells are profoundly inhibited at spot onset when their retinal inputs are discharging most vigorously. The lagged cells come out of the inhibition and begin to discharge as the retinal afferents decrease their firing level. Humphrey and Weller (1988b) subsequently provided anatomic evidence that X_L-cells are subject to feed-forward inhibition mediated by intrageniculate interneurons, which themselves have firing patterns similar to those of retinal afferents and nonlagged X-relay cells. It was thus proposed that the lagged cell's response to visual stimuli results from a two-step operation. First, the retinal signal is inverted by a geniculate interneuron that inhibits the lagged cell as the retinal afferent fires at stimulus onset. Second, the lagged cell begins to discharge as the afferent and interneuron decrease their firing. We suggest that this early inhibition and the response to its decrease are responsible for the absolute phase shift in lagged cells. The transformation between retinal afferents and lagged cells may be described by a linear system which includes *1*) inversion, corresponding to the feed-forward inhibition; *2*) differentiation, giving the phase shift, and corresponding to the response to the decrease in inhibition, and *3*) low-pass stages. Our data are consistent with such a model but are inadequate for derivation of the model parameters, which would require simultaneous recording experiments like those of Mastronarde (1987b).

The increased phase latency of lagged cells is more difficult to associate with mechanisms but may reflect low-pass filtering. The small but consistent deviation toward convexity we observed in the response phase versus temporal frequency data suggests the existence of low-pass mechanisms. The process that produces the additional latency of ~70 ms (beyond the 60-ms latency seen in nonlagged cells) could involve integration needed to activate channels. In this regard, recent evidence suggests that the excitatory responses of lagged X- and Y-cells are mediated primarily by *N*-methyl-D-aspartate (NMDA) receptors. Heggelund and Hartveit (1989) report that activity in lagged cells, but not nonlagged cells, is reduced or abolished by the NMDA antagonist CPP. Nonlagged cells appear much more sensitive to non-NMDA antagonists. These data suggest a model in which non-NMDA receptors would convey the retinal signal to the nonlagged interneuron, providing early inhibition onto the lagged geniculate relay cell. NMDA receptor–mediated excitatory synapses directly onto the lagged cell would be ineffective until unblocked, perhaps by calcium spiking or by removal of inhibition coupled with small amounts of non-NMDA–mediated depolarization. Our data on timing argue that activation of the excitatory mechanism must be tied to some form of inhibitory

rebound. The interaction of this rebound process and the time course of the NMDA receptor–mediated potentials (Forsythe and Westbrook 1988) may require the sorts of integration times we have observed in lagged cells.

One of the lessons from our work on lagged geniculate cells involves the role of inhibition in the central nervous system. Inhibition does not simply turn these cells off but generates a phase shift. The modulation of the magnitude of the signal conveyed by a lagged cell may be a minor consequence of the inhibition with the major consequence being the phase shift. The static view of inhibition as acting mainly on firing rates must be replaced, at least in this instance, by a dynamic view, where its role is to shape the responses of cells in time. Inhibition may play a similar role in other domains and in other systems, shaping responses rather than vetoing them (Dykes et al. 1984; Hicks et al. 1986; Srinivasan et al. 1982).

A role for lagged and nonlagged responses in generating cortical direction selectivity

Most lagged and nonlagged geniculate neurons project to visual cortex (Humphrey and Weller 1988a; Mastronarde 1987a). An important question addressed in this last section is whether the timing differences between these afferents might contribute to the generation of response properties in cortical cells.

Recently, attention has been focused on a class of models for psychophysical and visual cortical direction selectivity. These models require the interaction of at least two inputs that are not direction selective but which carry signals that are about one-quarter cycle out of phase with each other in space and in time; this is known as *spatiotemporal quadrature* (Adelson and Bergen 1985; van Santen and Sperling 1985; Watson and Ahumada 1985).

Spatial quadrature is easily obtained from pairs of neurons whose receptive fields are offset from each other or in cortex from odd- and even-symmetric receptive fields (Pollen and Ronner 1981). The physiological substrate for temporal quadrature is much less clear, but cortical cells do obtain inputs that are in temporal quadrature. Movshon et al. (1978), Reid et al. (1987), and McLean and Palmer (1989) reported continuous variations in response phase across receptive fields of single cortical neurons that correlated with the cells' direction selectivity. Because a quarter cycle is equivalent to delays from 25 to 250 ms in the range of frequencies from 10 to 1 Hz, somewhat complicated mechanisms might be needed to provide temporal quadrature. However, lagged and nonlagged geniculate cells respond about one-quarter cycle apart at low temporal frequencies, and it is tempting to speculate that they provide the temporal quadrature inputs to direction-selective cells in area 17.

A simple model is presented in Fig. 14*A*, wherein X_L- and X_N-cells converge in cortex to produce direction selectivity. We simulated this model by providing data from lagged and nonlagged cells and adding their estimated responses to drifting sine-wave gratings. The model was entirely linear and rectification was ignored. Our purpose was simply to investigate the potential of a scheme that combines these two afferent cell types. In Fig. 14*A*, we illustrate excitatory synapses in the nonlagged pathway and one inhibitory synapse in the lagged pathway. Because of the linearity used in the simulations, whether the synapses are excitatory or inhibitory does not affect the responses, except to reverse preferred and nonpreferred directions. The spatial assumptions involved offsetting the receptive fields

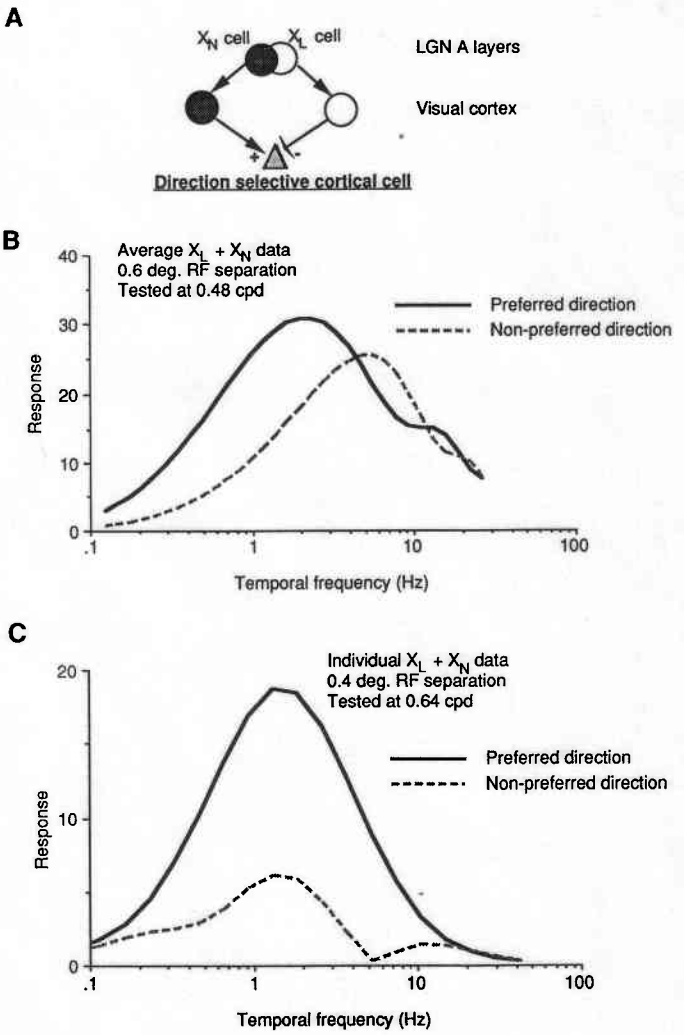

FIG. 14. *A*: lagged and nonlagged geniculate cells with neighboring receptive fields project to cortex where they are hypothesized to converge on cells to generate direction selectivity. Geniculate inputs may be relayed through cortical cells with little direction selectivity. One of the pathways onto the direction-selective cortical cell may involve inhibitory synapses, which we indicate for the lagged path. *B*: simulation based on the scheme shown in *A*, using the average values of relevant parameters from the X_N and X_L data compiled in this study (see Tables 1 and 2). Solid and dashed lines show the responses that would be obtained for opposite directions of movement. At temporal frequencies around 1 Hz, the hypothetical cell would be direction selective. Above 3 Hz, both directions give similar responses. Direction preference reverses periodically as the relative phase increases. *C*: simulation like that in *B* but based on 2 cells recorded next to each other in the LGN. One was an ON-center X_L-cell with a phase latency of 104 ms and an absolute phase of 0.098 cycles. The other cell was an OFF-center X_N with a latency of 87 ms and an absolute phase of −0.085 cycles. These cells therefore maintained a relative phase near one-quarter cycle over a wide range of temporal frequencies. The hypothetical cortical cell thus maintains a strong direction bias over a wide range of frequencies. Note that it is not important for the model that the 2 geniculate inputs had opposite center signs. Optimal spatial and temporal frequencies were 0.7 cpd and 1.3 Hz for the X_L-cell and 0.6 cpd and 1.5 Hz for the X_N-cell.

of the geniculate units by a distance that was approximately one-quarter of their spatial wavelengths (the reciprocal of their optimal spatial frequencies). Responses were simulated for test gratings of various spatial and temporal frequencies drifting in each direction along the axis through the receptive-field centers. For the illustrations in Fig. 14*B* and *C*, we chose a spatial frequency close to the optimum (spatial aliasing occurs in the simulations but may be avoided with odd and even cortical receptive fields).

Figure 14*B* illustrates the results of a simulation based on the averaged parameters from the X_L- and X_N-cell samples. The solid and dashed lines show the response amplitude versus temporal frequency for movement in opposite directions. The simulated cortical cell would be somewhat direction selective up to ~3 Hz, including at the optimal frequency of ~2 Hz. However, the latency difference between the inputs means that temporal quadrature is not maintained. Aliasing thus occurs at high frequencies, as the curves cross each other at intervals of ~7 Hz (the latency difference is 69 ms, which produces a half cycle of phase difference every 7.2 Hz). However, the cell would have little direction preference above 4 Hz, even though it continues to respond well beyond 10 Hz. This is because of the tuning properties of the inputs; lagged cells respond poorly relative to nonlagged cells at higher temporal frequencies.

Pairs of lagged and nonlagged cells could be chosen that produced stronger direction selectivity. Figure 14*C* shows the responses in each direction generated by combining data from two cells that were recorded next to each other in the LGN (whether this anatomic contiguity has any relevance for cortical direction selectivity is unknown). In this case direction selectivity is maintained across a broad range of frequencies. These two cells had latencies that differed by only 17 ms, and their absolute phase difference (0.18 cycles) was such that aliasing was avoided until 19 Hz, when little response remained.

These simulations verify that, assuming appropriate connections in cortex, direction-selective cells could be generated from inputs driven by lagged and nonlagged geniculate cells that are bidirectional but in spatiotemporal quadrature. Cortical receptive fields may show signs of such convergent inputs in subzones with differing absolute phases, latencies, and temporal resolutions.

We thank C. Lucci for writing most of the stimulus generation and data collection software. N. Swindale generously provided analysis and graphics software.

This work was supported by National Institutes of Health Grants EY-06034 to A. B. Saul and EY-06459 and RR-05416 to A. L. Humphrey.

Address for reprint requests: A. Saul, Dept. of Neurobiology, Anatomy, and Cell Science, University of Pittsburgh School of Medicine, 3550 Terrace St., Pittsburgh, PA 15261.

Received 11 October 1989; accepted in final form 16 February 1990.

REFERENCES

ADELSON, E. H. AND BERGEN, J. R. Spatiotemporal energy models for the perception of motion. *J. Opt. Soc. Am.* 2: 284–299, 1985.

BISHOP, P. O., KOZAK, W., AND VAKKUR, G. J. Some quantitative aspects of the cat's eye: axis and plane of reference, visual field co-ordinates and optics. *J. Physiol. Lond.* 163: 466–502, 1962.

BLAKE, R. AND CAMISA, J. Temporal aspects of spatial vision in the cat. *Exp. Brain Res.* 28: 325–333, 1977.

CLELAND, B. G., DUBIN, M. W., AND LEVICK, W. R. Sustained and transient neurones in the cat's retina and lateral geniculate nucleus. *J. Physiol. Lond.* 217: 473–496, 1971.

DERRINGTON, A. M. AND FUCHS, A. F. Spatial and temporal properties of X and Y cells in the cat lateral geniculate nucleus. *J. Physiol. Lond.* 293: 347–364, 1979.

DYKES, R. W., LANDRY, P., METHERATE, R., AND HICKS, T. P. Functional role of GABA in cat primary somatosensory cortex: shaping receptive fields of cortical neurons. *J. Neurophysiol.* 52: 1066–1093, 1984.

ENROTH-CUGELL, C. AND ROBSON, J. G. The contrast sensitivity of retinal ganglion cells of the cat. *J. Physiol. Lond.* 187: 517–552, 1966.

FORSYTHE, I. D. AND WESTBROOK, G. L. Slow excitatory postsynaptic currents mediated by *N*-methyl-D-aspartate receptors on cultured mouse central neurones. *J. Physiol. Lond.* 396: 515–533, 1988.

HAMMOND, P. Inadequacy of nitrous oxide/oxygen mixtures for maintaining anesthesia in cats: satisfactory alternative. *Pain* 5: 143–151, 1978.

HEGGELUND, P. AND HARTVEIT, E. Lagged and non-lagged X-cells in the cat lateral geniculate nucleus receive retinal input through different glutamate receptors. *Soc. Neurosci. Abstr.* 15: 175, 1989.

HICKS, T. P., METHERATE, R., LANDRY, P., AND DYKES, R. W. Bicuculline-induced alterations of response properties in functionally identified ventroposterior thalamic neurones. *Exp. Brain Res.* 63: 248–264, 1986.

HOCHSTEIN, S. AND SHAPLEY, R. M. Quantitative analysis of retinal ganglion cell classifications. *J. Physiol. Lond.* 262: 237–264, 1976.

HOFFMAN, K.-P., STONE, J., AND SHERMAN, S. M. Relay of receptive-field properties in dorsal lateral geniculate nucleus of the cat. *J. Neurophysiol.* 35: 518–531, 1972.

HUMPHREY, A. L., SUR, M., UHLRICH, D. J., AND SHERMAN, S. M. Projection patterns of individual X- and Y-cell axons from the lateral geniculate nucleus to cortical area 17 in the cat. *J. Comp. Neurol.* 233: 159–189, 1985.

HUMPHREY, A. L. AND WELLER, R. E. Functionally distinct groups of X-cells in the lateral geniculate nucleus of the cat. *J. Comp. Neurol.* 268: 429–447, 1988a.

HUMPHREY, A. L. AND WELLER, R. E. Structural correlates of functionally distinct X-cells in the lateral geniculate nucleus of the cat. *J. Comp. Neurol.* 268: 448–468, 1988b.

IKEDA, H. AND WRIGHT, M. J. Receptive field organization of 'sustained' and 'transient' retinal ganglion cells which subserve different functional roles. *J. Physiol. Lond.* 227: 769–800, 1972.

LEE, B. B., ELEPFANDT, A., AND VIRSU, V. Phase of responses to moving sinusoidal gratings in cells of cat retina and lateral geniculate nucleus. *J. Neurophysiol.* 45: 807–817, 1981.

LEHMKUHLE, S., KRATZ, K. E., MANGEL, S. C., AND SHERMAN, S. M. Spatial and temporal sensitivity of X- and Y-cells in dorsal lateral geniculate nucleus of the cat. *J. Neurophysiol.* 43: 520–541, 1980.

MALPELI, J. G. Activity of cells in area 17 of the cat in absence of input from layer A of lateral geniculate nucleus. *J. Neurophysiol.* 49: 595–610, 1983.

MASTRONARDE, D. N. Two classes of single-input X-cells in cat lateral geniculate nucleus. I. Receptive-field properties and classification of cells. *J. Neurophysiol.* 57: 357–380, 1987a.

MASTRONARDE, D. N. Two classes of single-input X-cells in cat lateral geniculate nucleus. II. Retinal inputs and the generation of receptive-field properties. *J. Neurophysiol.* 57: 381–413, 1987b.

MASTRONARDE, D. N. Branching of X and Y functional pathways in cat lateral geniculate nucleus. *Soc. Neurosci. Abstr.* 14: 309, 1988a.

MASTRONARDE, D. N. *Divergence of Retinal Input into Functionally Different Cell Classes in the Cat's Lateral Geniculate Nucleus* (PhD dissertation). Boulder, CO: Univ. of Colorado, 1988b.

MCLEAN, J. AND PALMER, L. A. Contribution of linear spatiotemporal receptive field structure to velocity selectivity of simple cells in area 17 of cat. *Vision Res.* 29: 675–679, 1989.

MOVSHON, J. A., THOMPSON, I. D., AND TOLHURST, D. J. Spatial summation in the receptive fields of simple cells in the cat's striate cortex. *J. Physiol. Lond.* 283: 53–77, 1978.

NELDER, J. A. AND MEAD, R. A simplex method for function minimization. *Computer Journal* 7: 308, 1965.

POLLEN, D. A. AND RONNER, S. F. Phase relationship between adjacent simple cells in the visual cortex. *Science Wash. DC* 212: 1409–1411, 1981.

PRESS, W. H., FLANNERY, B. P., TEUKOLSKY, S. A., AND VETTERLING, W. T. *Numerical Recipes: The Art of Scientific Computing.* Cambridge, UK: Cambridge Univ. Press, 1986.

REID, R. C., SOODAK, R. E., AND SHAPLEY, R. M. Linear mechanisms of directional selectivity in simple cells of cat striate cortex. *Proc. Natl. Acad. Sci. USA* 84: 8740–8744, 1987.

RODIECK, R. W. Quantitative analysis of cat retinal ganglion cell response to visual stimuli. *Vision Res.* 5: 583–601, 1965.

SANDERSON, K. J. The projection of the visual field to the lateral geniculate and medial interlaminar nuclei in the cat. *J. Comp. Neurol.* 143: 101–118, 1971.

SAUL, A. B. AND HUMPHREY, A. L. Temporal response properties of lagged and non-lagged cells in the cat lateral geniculate nucleus. *Soc. Neurosci. Abstr.* 14: 39, 1988.

SAUL, A. B. AND HUMPHREY, A. L. Phase differences in the cat LGN and cortical direction selectivity. *Soc. Neurosci. Abstr.* 15: 1394, 1989.

SESTOKAS, A. K. AND LEHMKUHLE, S. Visual response latency of X- and Y-cells in the dorsal lateral geniculate nucleus of the cat. *Vision Res.* 26: 1041–1054, 1986.

SHAPLEY, R. M. AND VICTOR, J. D. The effect of contrast on the transfer properties of cat retinal ganglion cells. *J. Physiol. Lond.* 285: 275–298, 1978.

SHAPLEY, R. M. AND VICTOR, J. D. How the contrast gain control modifies the frequency responses of cat retinal ganglion cells. *J. Physiol. Lond.* 318: 161–179, 1981.

SHERMAN, S. M. Functional organization of the W-, X-, and Y-cell pathways: a review and hypothesis. In: *Progress in Psychobiology and Physiological Psychology,* edited by J. M. Sprague and A. N. Epstein. New York: Academic, 1985, vol. 11, p. 233–314.

SO, Y. T. AND SHAPLEY, R. Spatial tuning of cells in and around lateral geniculate nucleus of the cat: X and Y relay cells and perigeniculate interneurons. *J. Neurophysiol.* 45: 107–120, 1981.

SRINIVASAN, M. V., LAUGHLIN, S. B., AND DUBS, A. Predictive coding: a fresh view of inhibition in the retina. *Proc. R. Soc. Lond. B Biol. Sci.* 216: 427–459, 1982.

STONE, J. AND DREHER, B. Projection of X- and Y-cells of the cat's lateral geniculate nucleus to areas 17 and 18 of visual cortex. *J. Neurophysiol.* 36: 551–567, 1973.

STONE, J., DREHER, B., AND LEVENTHAL, A. Hierarchical and parallel mechanisms in the organization of visual cortex. *Brain Res. Rev.* 1: 345–394, 1979.

TOLHURST, D. J. Separate channels for the analysis of the shape and movement of a moving visual stimulus. *J. Physiol. Lond.* 231: 385–402, 1973.

TOLHURST, D. J., WALKER, N. S., THOMPSON, I. D., AND DEAN, A. F. Nonlinearities of temporal summation in neurones in area 17 of the cat. *Exp. Brain Res.* 38: 431–435, 1980.

VAN SANTEN, J. P. H. AND SPERLING, G. Elaborated Reichardt detectors. *J. Opt. Soc. Am.* 2: 300–321, 1985.

WATSON, A. B. AND AHUMADA, A. J., JR. Model of human visual-motion sensing. *J. Opt. Soc. Am.* 2: 322–342, 1985.

WILSON, P. D., ROWE, M. J., AND STONE, J. Properties of relay cells in the cat's lateral geniculate nucleus. A comparison of W-cells with X- and Y-cells. *J. Neurophysiol.* 39: 1193–1209, 1976.